Alkynylgold(I) C 3 -Chiral Concave Complexes: Aggregation and Luminescence

Jing Zhang, Astrid Schaly, Jean-Claude Chambron, Bruno Vincent, Nathalie Zorn, Emmanuelle Leize-Wagner, Marion Jean, Nicolas Vanthuyne

Alkynylgold(I) C_3-Chiral Concave Complexes: Aggregation and Luminescence

Jing Zhang,[a] Astrid Schaly,[b] Jean-Claude Chambron,[a,b]* Bruno Vincent,[a] Nathalie Zorn,[c] Emmanuelle Leize-Wagner,[c]* Marion Jean,[d] and Nicolas Vanthuyne[d]*

Dedication ((optional))

[a] J. Zhang, Dr. J.-C. Chambron, Dr. B. Vincent
Institut de Chimie de Strasbourg, UMR 7177 CNRS
Université de Strasbourg
1, rue Blaise Pascal, BP 296 R8, 67008 Strasbourg, France
E-mail: jcchambron@unistra.fr

[b] Dr. A. Schaly, Dr. J.-C. Chambron
Institut de Chimie Moléculaire de l'Université de Bourgogne, UMR 6302 CNRS
Université Bourgogne Franche-Comté
9, avenue Alain Savary, 21078 Dijon, France

[c] N. Zorn, Dr. E. Leize-Wagner
Chimie de la Matière Complexe, UMR 7140 CNRS
Université de Strasbourg
4, rue Blaise Pascal, 67070 Strasbourg, France
leize@unistra.fr

[d] M. Jean, Dr. N. Vanthuyne
Aix Marseille Univ, CNRS,
Centrale Marseille, iSm2,
Marseille, France
nicolas.vanthuyne@univ-amu.fr

Supporting information for this article is given via a link at the end of the document.

Abstract: Chiral gold(I) acetylide trinuclear complexes **1** - **3** based on the cyclotribenzylene platform and terminal PR_3 ligands (R = Ph, Et, and Cy, respectively), were characterized and their light emission studied. They exhibited long-lived blue phosphorescence in $CHCl_3$ and a weak fluorescence in the UV. In MeOH/$CHCl_3$ mixtures of > 1:1 volume ratio, **1** and **2** exhibited a new emission band at *ca* 540 nm that developed at the expense of the UV emission. DLS studies demonstrated the presence of molecular aggregates of Ø 30 - 80 nm. The green emission observed in MeOH-rich solvent mixtures was therefore induced by aggregation, and could originate from Au···Au interactions. The AIE spectrum of **3** was observed only in solutions containing 99% of MeOH, and correlated with its solid state emission. The AIE profiles of the enantiomers of **1** differed from that of *rac*-**1**, suggesting that the latter is a true racemate.

Introduction

Gold(I) alkynyl complexes with phosphine or isonitrile ancillary ligands, since the first report in 1959,[1] received increasing attention after their unique photophysical properties,[2-19] coupled to the possibility of intramolecular aurophilic interactions in polynuclear complexes,[20-26] and intermolecular Au···Au short contacts in the solid state[5,27-29] or in supramolecular assemblies[30-33] had been recognized.[34,35] The interest in these compounds was currently raised by the applications[36] of their luminescence properties to the development of materials for (opto)electronics,[37,38] sensing,[22,25,26,33,39,40] and cellular imaging.[41,42]

We have been interested for several years in the chemistry of the cyclotribenzylenes (CTB), which are concave, C_3-symmetric cyclophanes.[43-46] These compounds have been mainly used in the construction of cage-like molecules, the cryptophanes, which were invented by Collet in the early eighties.[47] These families of compounds displayed very original receptor properties, as they were shown to be able to host a broad range of guests from atoms (Xe), soft metal cations (Cs^+), to small molecules (alkanes, haloalkanes), and alkylammonium cations.[48,49] The main driving forces are converging van der Waals / cation-π interactions, but hemicryptophanes offered the possibility to introduce hydrogen bond donors in the architecture of CTB-based receptors and increase the diversity of guests.[50] In the last 20 years, self-assembly approaches to cryptophanes, by coordination bonds[51-53] and dynamic covalent chemistry,[54,55] were developed. In this context, we recently reported on the stereoselective preparation of chiral metallo-organic cryptophanes by face-to-face dimerization of carbonitrile-substituted CTBs using $[M(dppp)]^{2+}$ metal complex fragments as assembling species, in which M = Pd or Pt, and dppp is 1,3-bis(diphenylphosphino)propane).[56,57] The carbonitrile and acetylide ligands subunits are isoelectronic and isosteric. At the time we started our investigations, alkynyl-substituted CTBs were known, but not used for the preparation of organometallic derivatives.[58-61] We wondered therefore if it would be possible to prepare metallo-cryptophanes by self-dimerization of gold(I) alkynyl CTBs in order to: (i) Expand the diversity of methods used for the assembly of metal cation-incorporating cryptophanes, and (ii) take advantage of the luminescence of the gold(I) alkynyl complex subunits to create original luminescent cryptophane-like receptors.[61-65]

We now report the results that we obtained with the three chiral gold(I) acetylide trinuclear CTB complexes bearing phosphine ancillary ligands **1** - **3** (Figure 1), which were prepared from ethynyl-substituted CTB(H,C_2H). We show that the complexes were endowed with the expected photophysical properties, while they did not dimerize into metallo-cryptophanes in solution. However, we found that the gold(I) alkynyl CTBs formed nanoscopic aggregates in $CHCl_3$/MeOH mixtures at high methanol volumetric ratio. This phenomenon was accompanied by changes in the electronic absorption spectra and a switch of the UV fluorescence to the emission of a green light, which could result from intermolecular aurophilic interactions within the aggregates. In the case of complex **1**, which was resolved into its enantiomers by chiral HPLC, the aggregation was also monitored by electronic circular dichroism. Interestingly, the evolution of the intensity of the aggregation induced emission (AIE) with the solvent composition of the separated enantiomers differed from that of the racemic form of **1**, indicating that the aggregates of the latter are true racemates.

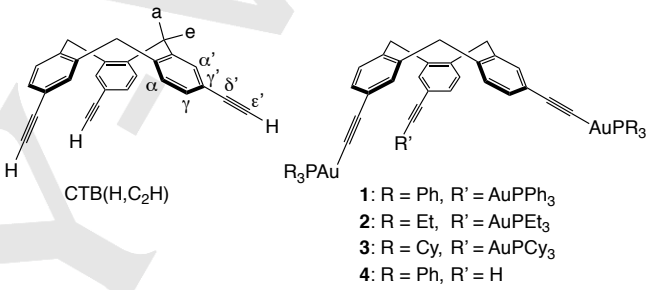

Figure 1. Structural formulae of the CTBs of this study.

Results and Discussion

Synthesis, purification, resolution, and characterization of the complexes. CTB(H,C_2H) was obtained in two steps in 80% overall yield from CTB(H,OTf)[56] by Sonogashira cross-coupling with trimethysilylacetylene using $[Pd(PPh_3)_2Cl_2]$ as catalyst and Et_3N as base, followed by removal of the TMS protecting groups with tetrabutylammonium fluoride.[66] The trinuclear gold complexes CTB(H,C_2AuPR_3) (R = Ph: **1**; R = Et: **2**, and R = Cy: **3**), were prepared by nucleophilic substitution of $[Au(PR_3)Cl]$ (R = Ph, Et, and Cy) in the presence of sodium methoxide.[67,68] They were isolated in 60, 68, and 72% yields, respectively. **1** was also prepared from $[CTB(H,C_2Au)]_n$, a poorly soluble polymer intermediate,[21,69] obtained by reaction of CTB(H,C_2H) with $[Au(SMe_2)Cl]$ in the presence of sodium acetate. Scavenging of the polymer with the stoichiometric amount of triphenylphosphine at room temperature afforded **1** in 78% yield after purification by controlled precipitation. Noteworthy, **2** could not be obtained using these milder reaction conditions, a fact in agreement with literature observations indicating that the use of alkyl substituted phosphine ligands did not cleanly depolymerize gold(I) acetylide polymers.[40] This route was therefore not further explored.

Racemic CTB(H,C_2H) and **1** were resolved by HPLC on chiral stationary phase using hexane/ethanol/dichloromethane mixtures as eluent (Figures S1, S3, and S5). Whereas CTB(H,C_2H) was perfectly stable in these conditions and could

be resolved into its enantiomers with > 99.5 ee, we observed that **1** underwent noticeable degradation, hence the relatively low yields of optically pure material collected. In the course of the resolution of **1** we isolated small amounts of the asymmetric CTB **4**, which we had not detected in the ^{1}H NMR spectrum of the precipitated material. Hence, it could have resulted from the partial degradation of **1** on the column. The kinetics parameters for the enantiomerisation of (+)-CTB(H,C_2H) in dichloromethane were determined: At 40 °C, k_{en} = 1.396 10^{-6} s^{-1}. This value corresponds to a half-life of 69 hours. The energy barrier of enantiomerisation is 111.9 kJ mol^{-1} (26.8 kcal mol^{-1}), which is in keeping with the values reported for other CTBs, confirming that these value are not very much sensitive to the nature of the substituents of the CTB rim.[47] The values of the specific rotation $[\alpha]_D^{25}$ obtained by polarimetry were –634 for the first eluted enantiomer and +634 for the second eluted enantiomer of CTB(H,C_2H). Their absolute value decreased to *ca* 440 for the enantiomers of **1**, which were eluted in the same order (Table S1).

The gold-phosphine CTBs were characterized by ^{1}H, ^{13}C, and ^{31}P NMR spectroscopy (Figures S7 - S38), Electrospray ionization time-of-flight mass spectrometry; Figures S39 - S48), IR spectroscopy, and elemental analyses. Upon metallation of CTB(H,C_2H), the singlet of the alkynyl proton at 3.02 ppm gradually disappeared, providing a convenient method for monitoring the reaction by ^{1}H NMR spectroscopy. Addition of a counter-solvent (cyclohexane or methanol) into dichloromethane solutions of the crude products allowed us to isolate the gold complexes in acceptable yields and purity, and was preferred to purification by column chromatography, our attempts showing marks of decomposition, as noted in the literature.[33] The complexes were air stable and soluble in chlorinated solvents such as CH_2Cl_2 and $CHCl_3$. The ^{1}H NMR spectra of CTB(H,C_2H) and its complexes showed the typical pairs of doublets for the diastereotopic axial (a) and equatorial (e) protons of the methylene bridges,[47] as well as the classical patterns of the α, γ and α' protons of singly γ'-C substituted CTBs. The trisubstitution of the *C*$_3$-symmetric CTB(H,C_2H) was attested by the simple NMR patterns observed. Complexation induced shifts (CIS) are lower than 0.1 ppm in the case of **1**, but in the case of **2** and **3,** α-H and e-H are shielded by amounts ≤ – 0.12 and a-H by ≤ – 0.10 ppm. In addition, γ-H are also more and more shielded upon going from less (PPh_3) to more (PCy_3) electron donor phosphines. Strong downfield CIS are observed in the ^{13}C NMR spectra for the alkynyl δ'-C and ε'-C ($\delta \approx 104.4$ ppm;[70] $\Delta\delta$ = +21 ppm); of the CTB carbon atoms, γ'-C, which bears the alkynyl substituent, shows the highest CIS (~ +2.4 ppm). Therefore Au(I) coordination affects significantly only the C atoms of the C(γ')–C(δ')≡C(ε') bond sequence. The ^{31}P NMR spectra show, for the PR_3 ancillary ligands, singlets at 43 ppm for **1** (R = Ph),[40,71,72] at 37 ppm for **2** (R = Et),[29] and at 57 ppm for **3** (R = Cy),[6,73,74] in agreement with literature data. Because of the chirality of the CTB platform, the protons of the methylene groups of the PEt_3 ancillary ligands in **2** are diastereotopic and represent the AB part of an ABX_3 system. However, instead of the theoretical triplet, the methyl protons show two triplets that are separated by 18 Hz, which correspond to a $^3J_{H,P}$ coupling constant. The IR spectra of all the complexes showed the characteristic, but weak signal corresponding to $\tilde{\nu}_{C\equiv C}$ at ~ 2100 cm^{-1}, which did not significantly differ from the corresponding band in the spectrum of CTB(H,C_2H).

Investigations on the monomeric/dimeric nature of the complexes. As the complexes could form face-to-face dimers by interpenetration of the $AuPR_3$ metal complex fragments and the establishment of aurophilic interactions (Figure S49), we investigated their nuclearity by combining different techniques, in particular in the case of **1**, for which Au···Au interactions would be the most favored electronically. First, the ^{1}H NMR spectrum of **1** in $CDCl_3$ was recorded at four different concentrations, from 0.9×10^{-3} to 1.5×10^{-2} M (Figure S50). All the signals were sharp and well resolved in diluted conditions, while they broadened upon increasing the concentration. We did not observe any significant shift, whatever the signals considered, in the concentration range explored. Variable temperature experiments between 298 and 193 K were performed using CD_2Cl_2 solutions (Figure S51). At 298 K, the signals of the protons of the CTB moiety (α, α', γ, a and e-H) were sharp, whereas those of the triphenylphosphine ligands were relatively broad. However, the latter gradually sharpened upon decreasing the temperature down to 208 K. Meanwhile, the CTB signals increasingly broadened from 238 to 193 K, temperature at which the whole spectrum showed broad features. Interestingly, all the proton signals underwent weak upfield shifts upon temperature decrease, the chemical shift variations ranging, over the whole temperature interval, from – 0.03 ppm for α, α', γ, and e-H to – 0.07 and – 0.08 ppm for a-H and (o, o')-H, respectively.

Next, the starting CTB(H,C_2H) and the three complexes **1** - **3** were studied by diffusion ordered spectroscopy (DOSY; see Supporting Information, Section 4-4 p. 51, and Figures S52 - S58).[75] We assumed that all the CTBs formed cryptophane-like dimers, and compared the hydrodynamic volumes obtained by diffusion data (v_H) with the geometrical volumes (v_M). The overall shape of a cryptophane in general can be considered as that of an oblate spheroid. However, the shape of metallo-organic cryptophanes, whose bridging metal complex fragments contain large-size auxiliary ligands, could be closer to that of a cylinder. The geometrical characteristics of the virtual CTB dimers were estimated using CPK molecular models. The hydrodynamic radii r_H were obtained from the measured translational diffusion coefficients D_t, using the general Stokes-Einstein equation.[76] They were first optimized using an iterative procedure.[77] Then they were used to calculate the volume v_H of the sphere equivalent to the model of geometrical volume v_M. If the model was correct, v_M and v_H would be equal. The results are collected in Table S2. The case of CTB(H,C_2H) is particular, because it cannot dimerize into a cryptophane. Therefore, we placed two CTB(H,C_2H) molecules face-to-face and considered that the resulting virtual dimer could be viewed as a spheroid. The corresponding v_H/v_M ratio (0.6) was close to 0.5, in agreement with the monomeric nature of CTB(H,C_2H). Surprisingly, in the case of complex **3**, whose bulky PCy_3 ancillary phosphine ligands are likely to strongly disfavor Au···Au interactions for steric and electronic reasons,[33] the v_H/v_M ratio was 0.98 for the spheroid, whereas its value for the cylinder model (0.66) was closer to that expected for a monomer! In fact, because of the large size of PCy_3, the shape of the virtual dimer would significantly depart from the spheroid and be best described by the cylinder model. Incidentally, the spheroid model accounts well for the diffusion properties of monomeric **3**. For complex **2** with smaller PEt_3 ancillary ligands, the v_H/v_M ratios are 0.77 and 0.51 for the spheroid and cylinder models, respectively,

indicating that the spheroid better describes the behavior of **2** by comparison with **3**. These observations indicate that the differences between the spheroidal and cylindrical models arise from the interplay between the size of the phosphine ligands and the interpenetration of the CTBs in the virtual dimer, the latter minimizing the size variation on going from the CTB to the virtual dimer. In the case of **1**, the experiments were run at 0.9 mM and 10 mM concentrations. In diluted conditions, the v_H/v_M ratios were 0.78 and 0.53 for the spheroid and cylinder models, respectively, and in concentrated conditions the same ratios were 0.96 and 0.65. In dilute conditions, the corresponding v_H/v_M ratio of 0.53 would confirm that **1** is actually monomeric. Its increase to 0.65 at 10 mM concentration could attest to the presence of small amounts of dimer in fast exchange.

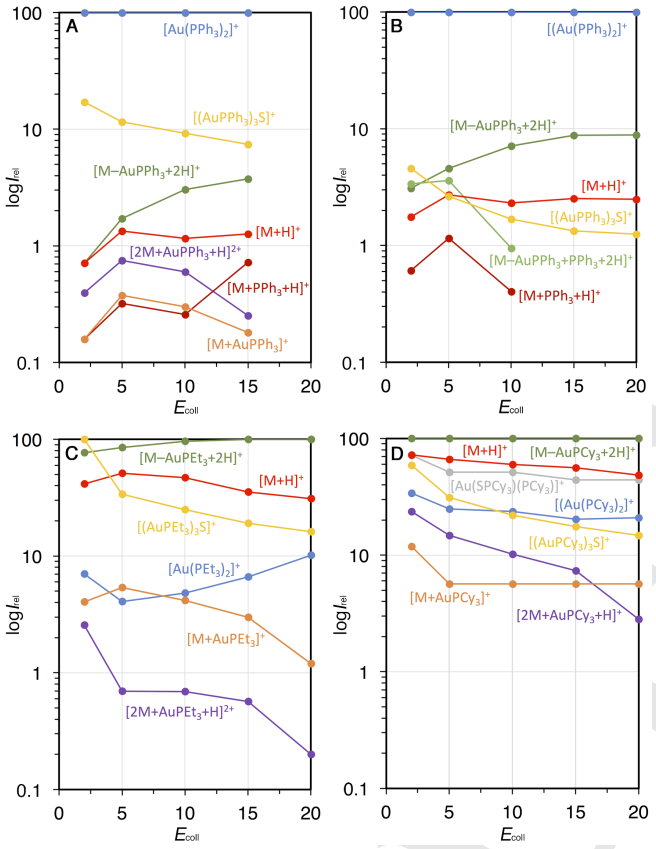

Figure 2. Evolution of the relative intensities (logarithmic scale) of the signals of the molecular species detected in the Electrospray ionization MS spectra of (A) **1**, (B) **4**, (C) **2**, and (D) **3**, as a function of E_{coll}.

The mass spectrometry data of the gold CTBs **1** - **4**, obtained by Electrospray ionization time-of-flight (Figures S39 - S48) are compared in Figure 2. The molecular peak $[M+H]^+$ could be observed only when the sample was injected in an acidic solvent mixture ($CHCl_3$/*i*PrOH/HCO_2H 1.00:0.99:0.01, v/v/v).[78] The relative intensity (I_r) of the $[M+H]^+$ signal of **1** at *m/z* = 1717.30 was very low (1.27% at E_{coll} = 15 eV and $c = 5 \times 10^{-5}$ M) with respect to the signal at *m/z* = 721.15 (I_r = 100%), which corresponds to $[Au(PPh_3)_2]^+$, by far the major species detected, the I_r of the others being less than a few percent, besides a signal at *m/z* = 1409.15 that we attributed to the known complex $[(AuPPh_3)_3S]^+$,[79-81] the origin of which being unclear. Other signals correspond to singly charged species, i.e. $[M–AuPPh_3+2H]^+$ (I_r = 3.76 at m/z = 1259.25), produced by the loss of a $[AuPPh_3]^+$ complex fragment followed by protonation of the alkynyl, $[M+PPh_3+H]^+$ (I_r = 0.72% at *m/z* = 1980.37), resulting from the coordination of an additional PPh_3 to one of the gold cations, and $[M+AuPPh_3]^+$ (I_r = 0.18%, *m/z* = 2176.36), in which the proton of $[M+H]^+$ has been replaced by the isolobal $[AuPPh_3]^+$ complex fragment. The mass spectrum obtained in the same conditions ($c = 5 \times 10^{-5}$ M, E_{coll} = 15 eV) for **2** showed very different characteristic features. The major signal (I_r = 100%) corresponded to the $[M–AuPEt_3+2H]^+$ species (*m/z* = 971.25), while the signal of $[Au(PEt_3)_2]^+$ (*m/z* = 433.15) had concomitantly decreased to I_r = 6.6%. The molecular peak corresponding to $[M+H]^+$ at *m/z* = 1285.29 had a much higher relative intensity (I_r = 31%) than the one observed in the case of **1**. The enhanced response of **2** by comparison with **1** could be due to the fact that triethylphosphine is more basic than triphenylphosphine. We also observed the signal of the sulfide-centered trinuclear gold complex $[(AuPEt_3)_3S]^+$ at *m/z* = 977.14 (I_r = 19%). Among those of weakest intensity, we noted a signal at *m/z* = 1599.34 (I_r = 3%), that could be attributed to $[M+AuPEt_3]^+$, the analogue of $[M+AuPPh_3]^+$. The features observed in the case of **2** in the same conditions ($c = 5 \times 10^{-5}$ M, E_{coll} = 15 eV) are even more pronounced when **3** is considered, e.g. major signal corresponding to $[M–AuPCy_3+2H]^+$ (m/z = 1295.53) accompanied by the signal of $[Au(PCy_3)_2]^+$ at m/z = 757.43 (I_r = 20.3%), and second more intense signal (I_r = 55.9%) due to $[M+H]^+$ (1771.72). The features observed for **4** are similar to those described in the case of **1**, but they are shifted to higher intensities. As shown in Figure 2, the intensity of the signal of $[M–AuPR_3+2H]^+$ increases with E_{coll} at low I_r levels for **1** and **4**, at a high I_r level for **2**, while being maximum for **3**. The intensities of the signal of $[M+H]^+$ also increase with E_{coll} at low I_r levels in the cases of **1** and **4**, whereas in the cases of **2** and **3** they slightly decrease at high I_r levels for $E_{coll} \geq 5$ eV.

Although of weak intensity, signals pertaining to doubly charged species were also observed in the mass spectra of the gold alkynyl CTBs **1**, **2**, and **3**. Noteworthy, such signals were not observed in the case of **4**. The signals of the species $[2M+AuPR_3+H]^{2+}$ appeared at *m/z* = 1947.33 (I_r = 0.25%) for R = Ph (**1**), at *m/z* = 1442.82 (I_r = 0.57%) for R = Et (**2**), and at m/z = 2010.32 (I_r = 7.34%) for R = Cy (**3**). The proportion of these doubly charged species decreased from $E_{coll} \geq 2$ eV in the case of R = alkyl. Moreover, the signals corresponding to the singly charged molecular species, $[M+H]^+$ and $[M+AuPR_3]^+$ were, to different extents, overlapped with those of the corresponding doubly charged species $[2M+2H]^{2+}$ and $[2M+2AuPR_3]^{2+}$ (see Figures S42, S44, S46, and S48 for $[M+H]^+/[2M+2H]^{2+}$). In fact, the ratio between the latter and the former (see Supporting Information, Section 4-5 p. 58, and Tables S3 and S4) depends on both the nature of the phosphine ligand and E_{coll}: In the case of **2**, the detail of the profile of the signal of $[M+H]^+$ shows that it corresponds only to a singly charged species whatever E_{coll}, whereas the profile of the signal of $[M+AuPEt_3]^+$ shows that the doubly charged species is present at E_{coll} = 2 and 5 eV, but disappears at $E_{coll} \geq 10$ eV. In the case of **1**, the signal of the doubly charged species $[2M+2H]^{2+}$ was overlapped with the signal of the singly charged species $[M+H]^+$ at $E_{coll} < 15$ eV, its proportion decreasing from 63% at E_{coll} = 2 eV to 12% at 10 eV. Moreover, the proportion of the adduct $[2M+2AuPPh_3]^{2+}$ predominates from E_{coll} = 2 eV to E_{coll} = 15 eV, being lower than the one of $[M+AuPPh_3]^+$ at E_{coll} = 20 eV. In the case of **3**, the

signal of the doubly charged species $[2M+2H]^{2+}$ was also overlapped with the signal of the singly charged species $[M+H]^+$, but at $E_{coll} \leq 5$ eV, its proportion decreasing from 21% at E_{coll} = 2 eV to 12% at 5 eV. We note that the profile of $[2M+2AuPCy_3]^{2+}$ can be seen at all E_{coll}. In summary, **1** exhibited the signals of all three doubly charged species with a higher propensity than **3**; **2** and **4** did not display the isotopic profile of $[2M+2H]^{2+}$, but **2** shows those of $[2M+AuPR_3+H]^{2+}$ and $[2M+2AuPR_3]^{2+}$. Therefore, an important issue is the chemical nature of the doubly charged species $[2M+2H]^{2+}$, $[2M+AuPR_3+H]^{2+}$, and $[2M+2AuPR_3]^{2+}$. The obvious possibility, which was brought up in the DOSY section, is that the dimers would result from face-to-face interpenetrated associations of the CTBs driven by aurophilic interactions. Indeed, such 1:1 associations have been observed by mass spectrometry in the case of C_3-symmetric trischelate cobalt complexes of triphenylphosphine gold alkynyl-functionalized bipyridine ligands. However, these observations were clearly supported by X-ray crystallography and ^{1}H NMR spectroscopy.[31] It must nevertheless be taken into account that all the complexes but **4** show the signals of the doubly-charged adducts $[2M+AuPR_3+H]^{2+}$ and $[2M+2AuPR_3]^{2+}$, which, unlike the case of $[2M+2H]^{2+}$, could form by bridging of the CTBs with an $[Au(PR_3)]^+$ complex fragment bound by Au···Au interactions. We also noted, in the case of **2**, the presence of very weak signals corresponding to the singly charged dimers $[2M–AuPEt_3+2H]^+$ at m/z = 2256.54 and $[2M–2AuPPh_3+3H]^+$ at m/z = 1941.48, resulting by the progressive replacement of $[AuPPh_3]^+$ fragments by H^+, whose evolution with E_{coll} has not been reported in Figure 2.

Table 1. Photophysical data of the complexes and the reference compounds in chloroform unless otherwise stated.

Compound	$\lambda_{max/sh}$ [nm] (ε_{max} [Lmol^{-1}cm^{-1}])	Cond.	$\lambda_{max/sh}$ [nm] (I_r [%])	Φ[a]	τ/µs
PhC_2AuPPh_3	239,[b] 269 (21000), 282 (20400) 291[sh,c]	Ar	361 (2.3), 381 (3.7), 420 (100), 442 (75), 445 (75), 458 (67),[sh] 478 (0.41)[sh,c]	0.0154[c]	
	238 (32000), 271 (19400), 284 (19300), 291 (11400)[sh,d,e]		419 (max)[d,f]	0.010[d,f]	6.0[d,f]
PhC_2AuPCy_3[g]	255 (14140), 267 (27440), 281 (28490), 290 (10190)[sh,d]	Ar	419 (max), 439, 446, 458, 483[sh,d]	0.08[d]	18.0[d]
$CTB(H,C_2H)$[c]	248,[b] 258 (39300), 282 (2300), 293 (1900)	Ar Air	306 306	n.d.	n.d.
1[c]	240,[b] 262 (52350), 276 (71250), 285 (86600), 298 (74500), 336 (2200)[sh]	Ar Air Solid	320 (3.76), 381 (10.4), 428 (100), 454 (84.7), 465[sh], 488[sh] 353 (58.9)[sh], 376 (100), 395 (93.3), 520 (8.6) 515	0.0246	29.5[h] 0.00075[i]
2[c]	248[sh],[b] 261 (34600)[sh], 273 (55000)[sh], 283 (69800), 295 (59600), 333 (2380)	Ar Air Solid	322 (4.65), 350 (10.2)[sh], 373 (17.9), 428 (100), 453 (76.8) 372 (100), 390 (83.8) 510	0.0246	31.8[h] 0.00069[i]
3[c]	250,[b] 261 (37700)[sh], 273 (60800)[sh], 282 (78700), 295 (68700), 332 (1200)	Ar Air Solid	350 (2.79), 383 (4.90), 428 (93.5), 454 (100), 530 (13.4) 368 (100), 380 (91.9), 532 (4.20) 412, 443, 475, 515	0.0636	36.8[h] 0.00084[i]

[a] Determined using PhC_2AuPPh_3 as reference. [b] Absorbances at wavelengths between 240 and 260 nm are not correct and were not given. [c] This work. [d] Solvent: CH_2Cl_2. [e] Ref. 4. [f] Ref. 2. [g] Ref. 6. [h] Observation at 460 nm. [i] Observation at 380 nm

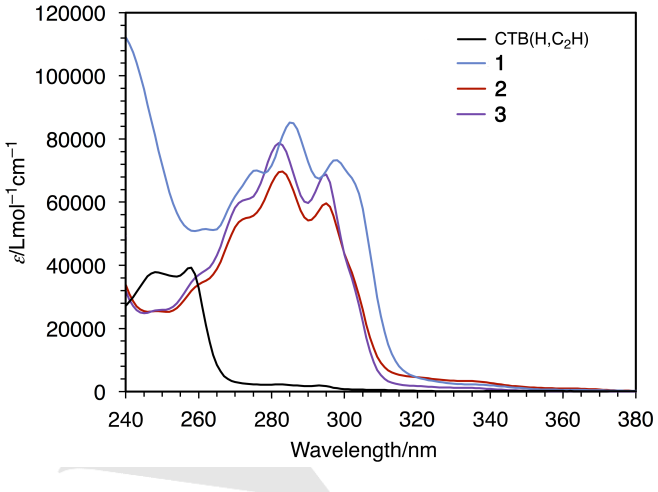

Figure 3. Electronic absorption spectra of 10^{-5} M solutions of $CTB(H,C_2H)$ and complexes **1** - **3** in $CHCl_3$.

Electronic spectroscopy of the complexes. The absorption and emission spectra of $CTB(H,C_2H)$ and the complexes **1** - **3** were investigated with 10^{-5} M $CHCl_3$ solutions, while the ECD and corresponding absorption spectra of the enantiomers of $CTB(H,C_2H)$ and **1** were recorded in CH_2Cl_2. The numeric data are collected in Table 1. As shown in Figure 3, $CTB(H,C_2H)$ shows strong absorptions in the UV region with maxima at 248 and 258 nm and a molar extinction coefficient of 39300 $M^{-1}cm^{-1}$ at this wavelength, which correspond to the B_{1u} transition of the CTB benzene rings. A much weaker absorption with maxima at 282 and 293 nm (ε = 1900 $M^{-1}cm^{-1}$) corresponds to the B_{2u} transition.[82] In their absorption spectra (Figures S60 - S62) the complexes show a few more-or-less resolved bands between 250 and 300 nm, with a maximum centered at *ca* 283 nm exhibiting high molar extinction coefficients, at *ca* 70000 $M^{-1}cm^{-1}$ for **2**, 79000 $M^{-1}cm^{-1}$ for **3**, and 87000 $M^{-1}cm^{-1}$ for **1**, and a slightly less intense band at ~ 295 nm, corresponding to the $S_0 \rightarrow S_1$ transition (Figure 3).[73] These bands are separated by vibrational spacings of 1531, 1437, and 1563 cm^{-1} for **1**, **2**, and **3**, respectively, which correspond to the stretching frequencies

of the aromatic carbon-carbon bonds.[3,7] The bands at 276 nm for **1**, and shoulders at 273 nm for **2** and **3** are separated from the respective maxima by 1144, 1295, and 1169 cm^{-1}. The absorption features above 250 nm were assigned primarily to the intraligand (IL) π-π* transition of the aryl Au(I) acetylide subunit,[2] possibly to the d_{π}(Au)-π* MLCT transition. In the case of complex **1**, the band below 260 nm was assigned to the IL transitions of the PPh_3 ligand,[83] as it is very much weaker for the other complexes. The molar extinction coefficient of **1** at 285 nm being about three times that of the reference complex PhC_2AuPPh_3, the three CTB chromophores are independent in the ground state. The low energy B_{2u} absorptions at 283 - 285 nm and 295 - 298 nm are considerably enhanced and, in the case of **1**, slightly red-shifted (3 - 5 nm), by comparison with the corresponding absorptions of free CTB(H,C_2H). Shifts of the absorption bands to lower energies upon alkynyl metalation have been noted in the literature and have been attributed to enhanced conjugation in the metal acetylide due to metal-to-ligand back donation to π*(C≡CAr).[68,70] The ECD spectrum of (–)-CTB(H,C_2H) showed a sequence of negative-positive-negative bands with maxima at λ = 237, 255, 285, and 294 nm, the sign inversion occurring at 258 and 266 nm, and is mirror-image of the spectrum of (+)-CTB(H,C_2H) (Figures 4 and S2). The ECDs of CTBs and compounds derived thereof often show bisignate bands in the 230-260 nm and 260-310 nm regions of the UV spectrum, which result from exciton coupling between the B_{1u} and B_{2u} transition dipole moments of the three benzene chromophores, respectively.[82,84,85] We tentatively assign to the B_{1u} transition the unsymmetrical couplet extending between 225 nm and 266 nm, and to the B_{2u} transition the singly signed band extending between 266 and *ca* 300 nm. In the same region, the ECD spectra of **1** (Figures 4 and S4) showed the same sequence of bands with maxima (or minima) at 242, 270, 288, and 304 nm with sign inversion at 264 and 274 nm. The sequence of signs for (–)-**1** and (+)-**1** was the same as for (–)-CTB(H,C_2H) and (+)-CTB(H,C_2H), respectively. The ECD spectra of complex **1** were shifted bathochromically by comparison with those of CTB(H,C_2H) by 6 - 8 nm if we refer to the respective positions of the sign inversion wavelengths, 10 nm if we refer to the low energy maximum of the B_{2u} band. In addition, the organometallic substituent-perturbed B_{2u} transition was considerably enhanced by comparison with the corresponding band in the spectra of CTB(H,C_2H), while the maximal $|\Delta\varepsilon|$ values of the high energy bisignate band of the B_{1u} transition were similar for CTB(H,C_2H) and its complex.

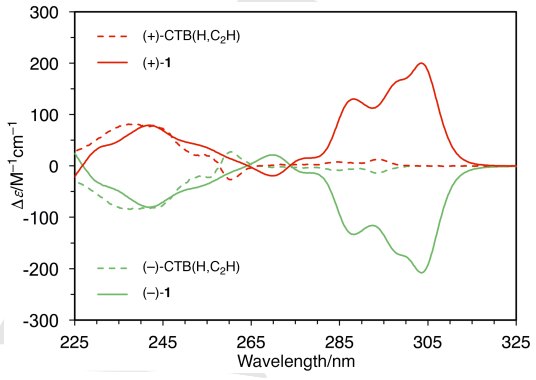

Figure 4. Superposition of the ECD spectra of the enantiomers of CTB(H,C_2H) and of complex **1** in CH_2Cl_2.

The electronic emission properties of the CTBs in $CHCl_3$ were investigated in aerated and degassed (Ar) conditions (Figures 5 and S63 - S68). CTB(H,C_2H) shows the strongest emission at 306 nm when excited at 260 nm, whether its solution is degassed or not. Upon excitation of degassed 10^{-5} M solutions in the strongest absorption band at 280 nm, **1** emitted blue light in the 300 - 600 nm range with a sharp maximum at 428 nm (relative intensity I_r = 100) appended with a broad band exhibiting a maximum at 454 nm (I_r = 84.7) and shoulders at *ca* 465 and 488 nm. We also note low intensity emission bands between 340 and 400 nm. The spectrum of **2** (Figure S67) displayed a very similar shape, whereas in the case of **3** (Figure S68), the band at 454 nm was enhanced by comparison with the peak at 428 nm, their relative intensities being inverted by comparison with the other CTBs, and PhC_2AuPPh_3 (Figure S64). However, the emission spectra of the three complexes produced by excitation in the lowest energy absorption band of the B_{2u} transition (300 nm) were very similar to each other, the residual high energy emission being of highest intensity in the case of **2**. Finally, when the complexes were excited in the residual absorption tail around 330 nm, their emission was switched to the low intensity features between 340 and 400 nm noted in the emission spectra obtained at higher excitation energies. For example, the high energy region of the emission spectrum of **1** showed a maximum at 381 nm, as well as a residual emission tail extending down to 600 nm (Figure 5a). These maxima were shifted to the blue by *ca* 8 nm in the case of **2**, whereas the high energy emission of **3** had a lower relative intensity (Figure 5b). As the emission spectra of **1** run by excitation at 280 and 300 nm showed two main emission bands (highest intensity at 428 nm and lowest energy at 454 nm) followed by a tail centered around 530 nm, three excitation spectra were collected by monitoring the emissions at 430, 455, and 530 nm, respectively (Figures 5 and S66). Interestingly, all three excitation spectra showed identical features, that is, a shoulder at 276 nm ($I_r \approx 92$), a maximum at 285 nm ($I_r \approx 100$), a lower energy maximum at 298 nm ($I_r \approx 90$), and a weak intensity very broad band tailing from 320 to 420 nm. Expectedly, there was no signal from the region corresponding to the excitation of the PPh_3 ligand. Otherwise, the shape and the maxima of the excitation spectra matched perfectly those of the absorption spectrum of **1**. The correspondence between the absorption and the excitation spectra of **2** and **3** was not so perfect.

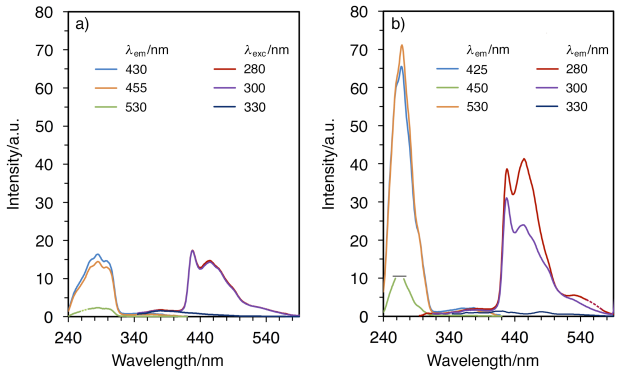

Figure 5. Excitation and emission spectra of 10^{-5} M solutions of the complexes (a) **1** and (b) **3** in degassed $CHCl_3$ at room temperature. Dotted and cut regions correspond to emission and excitation artifacts.

The high intensity emission bands at lower energy (*i.e.*, above 400 nm) were quenched when the solutions were not degassed, whereas the low intensity emission bands at higher energy (*i.e.*, below 400 nm; maxima between 368 and 376 nm) were still present in aerated solutions. The emission quantum yields of the complexes at $\lambda_{em} > 400$ nm were determined by comparison with PhC_2AuPPh_3 and found not to exceed 10%, and the corresponding lifetimes (Figures S69 - S74) were all around 30 μs. The lifetimes of the unquenched emission at $\lambda_{em} < 400$ nm were much shorter, *ca* 1 ns. The high intensity sharp luminescence with a maximum around 428 nm was not sensitive to the nature of the phosphine ligands. It had been assigned to a $T_1 \rightarrow S_0$ $\nu_{0\text{-}0}$ emission in related compounds.[6] The broad band at 454 nm with shoulders at lower energy corresponds to the envelope of the transitions to the higher order vibrational ground state levels (ν_1, ν_2, etc.), which were well resolved in the cases of the model complexes PhC_2AuPPh_3[2] and PhC_2AuPCy_3.[6] The corresponding vibrational spacings have been assigned to ground state phenyl ring deformation, symmetric phenyl ring stretch, and C≡C stretch. This emission corresponds to a phosphorescence, because it is quenched by oxygen, it is associated with a relatively large Stokes' shift (*ca.* 10^3 cm^{-1}), and it shows quite a long lifetime of *ca.* 30 μs. Noticeably, this magnitude lies in the upper range of those of literature gold(I) acetylide complexes.[6,15] Based on literature conclusions, the phosphorescence of **1** - **3** could be assigned to the metal-perturbed triplet π–π* transition involving the ArC ≡C^- phenylacetylide subunits.[5,6,86] Au(I) alkynyl complexes reported in the literature generally show exclusively phosphorescence, because of the high rate of the ISC process, which is facilitated by the spin orbit coupling induced by the heavy metal atom. The much weaker emission at high energy, which can be observed even in the presence of air by excitation at 330 nm, corresponds to a fluorescence, because of its insensitivity to oxygen, its small Stokes' shift with respect to the lowest energy absorption, and its short lifetime. There are several literature examples for which dual S_1/T_1 fluorescence has been pointed, and its origin clearly elucidated.[6,13-15,38,75] Reports on the emission properties of binuclear angular-shaped gold acetylide complexes of formula $[X(p\text{-}C_6H_4C_2AuPPh_3)_2]$ (X = CH_2, O, S, SO, and SO_2)[68,70] have noted a residual very weak fluorescence (*i.e.*, Φ = 0.4% for X = CH_2), which was turned into a strong phosphorescence at 77 K. Comparison of their luminescence properties to those of **1** in particular, is relevant, as they are made from two PhC_2AuPPh_3 subunits also held together by conjugation-breaking single atom units.

Moreover, we were intrigued by the fact that the phosphorescence of **1** - **3** was no longer observed upon excitation at longer wavelength (330 nm), while the fluorescence remained unchanged. The excitation wavelength dependence of the ratio between the phosphorescence and the fluorescence has been observed and investigated in the case of binuclear Au(I) alkynyl complexes of phenylene and alkynyl/phenylene-bridged diphosphine ligands.[13,14] By analogy with earlier observations on Os(II) complexes,[87] these observations were rationalized by invoking high lying S_n states with MLCT character, which transferred the excitation to T_1 via T_n states more efficiently than S_1 would do. In summary, the gold(I) alkynyl CTBs behave as three-channel light emitters, which can be controlled by changing the nature of the phosphine, the nature of the atmosphere (air or argon) and the excitation wavelength.

Studies on aggregation-induced emission.

Electronic spectroscopy (absorption, emission and ECD) studies in solvent mixtures of increasing polarity and hydrophilic character. The complexes of this study are not soluble in polar and/or hydrophilic solvents such as acetonitrile and methanol. Therefore, we used electronic spectroscopies, which allowed us to work with 10^{-5} M solutions to investigate the effect of the progressive change of the solvent properties. Increasing the $CH_3CN/CHCl_3$ ratio from 0:100 to 99:1 v/v produced a significant hyperchromism of all three major bands of **1** at 276, 285, and 298 nm (e.g., $\Delta\varepsilon/\varepsilon$ = + 22% for the 276 nm band), and a concomitant noticeable hypsochromic shift (*ca* 2 nm) of the absorption bands at 276 and 298 nm (Figure S75). By contrast, both residual absorbance between 312 and 350 nm and intensity of the weak emission at 530 nm observed by excitation at 330 nm decreased, the former by 23%, and the latter by 33% (Figure S76). The gradual addition of methanol in the same proportions as acetonitrile had very different effects (Figures 6 and S77). Increasing the $CH_3OH/CHCl_3$ ratio from 0:100 to 99:1 v/v produced a slight hyperchromism between 0 and 30% MeOH, followed by a strong decrease of the absorbance with band broadening and concomitant bathochromic shift above 60% MeOH. Overall, between 0 and 99% MeOH, the highest absorbance change reached 27% and the wavelength of the maximum of absorption shifted from 285 to 288 nm. Remarkably, the absorbance of the low energy tailing band increased in three steps: There were no changes from 0 to 30% methanol, then it increased first between 50 and 70% methanol, then at a higher rate between 70 and 90% methanol. Overall the absorbance at 330 nm was multiplied by nearly 3.5 between 0 and 90% methanol. This increase of absorbance is likely to be due to the combined Tyndall scattering and absorption of light by small size particles, a phenomenon that has been formalized by Mie.[88] We shall come back to this point in the section dealing with the ECD studies of solutions of optically-active **1** in $CHCl_3$/MeOH.

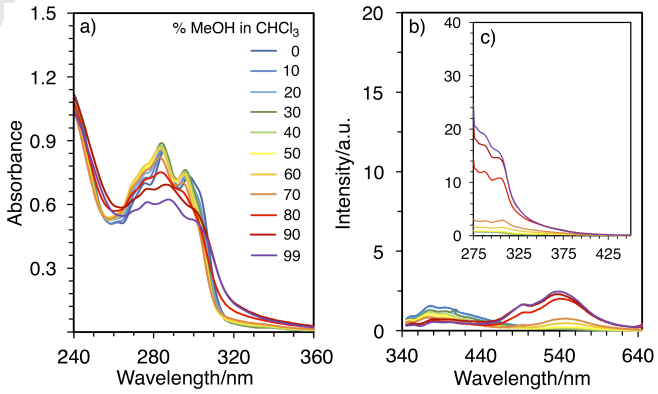

Figure 6. Evolution of the electronic (a) absorption, (b) emission, and (c) excitation spectra collected by observing the emission at 540 nm of 10^{-5} M solutions of fresh solutions of complex **1** in $CHCl_3$/MeOH mixtures under air at room temperature.

Drastic changes were observed when monitoring the emission collected upon excitation at 330 nm in aerated conditions (Figures 6b and S78). This excitation wavelength was chosen because it is located in the MeOH content-dependent band tail of the absorption spectrum. The intensity of the fluorescence band with maxima at 376 and 395 nm decreased

linearly while a new band with maxima at a much lower energy (494 and 539 nm) grew up progressively. The plot of the emission intensity at 540 nm versus the methanol/chloroform ratio (inset of Figure S78) showed features that were reminiscent of those previously noted for the variations of absorbance at 330 nm: No intensity change between 0 and 40% of methanol followed by a steady increase from 50 to 70%. A jump was then observed between 70 and 80%. The lowest energy emission maximum shifted significantly (13 nm) to shorter wavelengths from 550 nm for 50% MeOH to 537 nm for 99% MeOH. The shift was more pronounced above 70% MeOH. The evolution of the intensity of the tail of this band at 330 nm was the same as the evolution of the intensity of the emission at 540 nm upon excitation at 330 nm. The intensity ratios I_{542}^{99}/I_{376}^{0}, $I_{541}^{99}/I_{380}^{99}$, and I_{536}^{0}/I_{376}^{0} were 1.57, 4.40, and 0.08, respectively. The same experiments run several hours after the preparation of the solutions showed that the absorbance of the solutions containing 80 - 99% MeOH had decreased by comparison with those measured for the fresh solutions (Figure S79). The variations of the emission intensity of aged solutions of **1** around 545 nm (Figure S80) were similar to those observed with solutions examined immediately after preparation, but the intensity ratios I_{545}^{99}/I_{375}^{0}, $I_{539}^{99}/I_{380}^{99}$, and I_{534}^{0}/I_{376}^{0}, respectively 2.00, 5.48, and 0.09 were higher (Figure S81). Monitoring excitation spectra while observing the rise of the low energy emission (540 nm) showed the growth of bands at 288 and 308 nm, which coincide with the lower energy maxima of the absorption spectrum (Figures 6c and S82). In summary, the examination by electronic absorption and emission spectroscopies of dilute solutions of **1** in chloroform/methanol mixtures containing increasing proportions of methanol allowed us to discover that these solutions showed a two-phase behavior. The regular solution phase for methanol contents < 50%, and a new phase for methanol contents ≥ 60%.[89] Photographs of vials containing fresh and three-days old solutions of **1** in $CHCl_3$/MeOH mixtures are shown in Figures S85-S86. Control experiments showed that the excitation of a 10^{-5} M solution of CTB(H,C_2H) in $CHCl_3$/MeOH 1:99, in the same conditions as in pure $CHCl_3$, produced the same 306 nm emission in this solvent. Therefore, the new emission at 540 nm in MeOH-rich $CHCl_3$/MeOH mixtures is an intrinsic property of the gold(I) alkynyl CTBs, which was confirmed by subsequent experiments involving **2** - **4**.

$CHCl_3$/MeOH solutions of **2** prepared in aerobic conditions showed more marked time-dependent features. The electronic absorption spectra recorded immediately after preparation of the solutions did broaden and the maximum of absorption underwent a hypsochromic shift from 283 to 279 nm, but the corresponding optical densities did not change significantly (Figure S87). The evolution of the emission spectra of the fresh $CHCl_3$/MeOH solutions also differed from what was observed in the case of **1** (Figure S88). Upon increase of the MeOH content from 10 to 90% and finally 99%, the emission maximum at 371 nm shifted to the blue (365 nm at 99% MeOH), but its intensity did not decrease significantly, while the band at *ca* 540 nm was very weak (I_r = 0.04 at 99% MeOH). Nevertheless, the evolutions of the absorption and emission spectra after two days ripening in $CHCl_3$/MeOH mixtures (Figures S89-S90) resembled those observed for fresh solutions of **1**. Plotting the absorbance at 325 nm *vs.* the MeOH/$CHCl_3$ ratio showed that it also started to increase at 40% MeOH, the slope being then steeper between 60% and 90% MeOH. The emission spectra showed a steady decrease of the maximum at 372 nm, with a shift to 379 nm at high methanol content, to *ca* 10% of its initial value, while a new band centered around 550 nm developed. The plot of the emission intensity at 553 nm *vs* the MeOH/$CHCl_3$ ratio (insert of Figure S90) showed also a two-step increase: At first between 40% and 60% MeOH, then, at a higher rate, between 60 and 90%. Noticeably, the solution containing 99% MeOH did not seem to strictly follow the absorption and emission trends as the absorbance and emission intensity were slightly lower than those measured for 90% MeOH solutions. The intensity ratios I_{546}^{99}/I_{372}^{0}, $I_{546}^{99}/I_{379}^{99}$, and I_{546}^{0}/I_{372}^{0} were 0.42, 3.32, and 0.022.

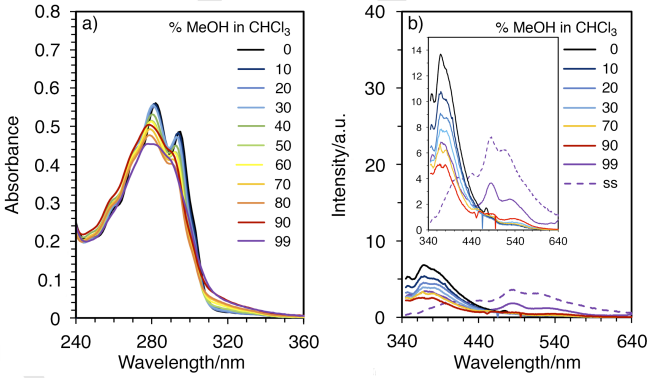

Figure 7. Evolution of the electronic (a) absorption and (b) emission spectra of 10^{-5} M solutions of complex **3** in $CHCl_3$/MeOH mixtures and in the solid state (ss) under air at room temperature. The intensities of the spectrum in solution have been multiplied by 10^5 by comparison with those in the solid state. Inset: Enlarged view of the emission spectra of **3**.

The absorbance changes of solutions of **3** in $CHCl_3$/MeOH mixtures examined two days after their preparation are shown in Figure S91. Increasing the methanol content up to 80% v/v shifted the maximum at 282 nm to 279 nm, while the other maximum (295 nm) also underwent a hypsochromic shift, with concomitant absorbance decrease and band broadening to such an extent that the lower energy maximum showed up as a shoulder at 80% MeOH. However, the overall variation of the optical density at the maximum (*ca* a 19% decrease), was the same as for **1**, and much lower than for **2** (ca 50%) between 100:0 and 10:90 $CHCl_3$/MeOH v/v. The optical density at 330 nm started to increase at 20% MeOH, at an earlier stage than for the two other complexes. The evolution of the emission spectra of 10^{-5} M solutions of **3** in $CHCl_3$/MeOH mixtures in aerobic conditions as a function of the volume ratio of MeOH is shown in Figure S92. The weak emission at 368 nm originally observed in $CHCl_3$ decreased upon gradual addition of MeOH, while the shoulder at lower energy emerged as a maximum at *ca* 381 nm for 30% of methanol. Contrary to the other complexes, the decrease of this emission band was not accompanied with the progressive growth of a new low energy band between 500 and 600 nm, but ultimately (at 99% MeOH) led to the sudden apparition of bands at 485 and 529 nm, the shape of which differed from the band observed in this region for **1** and **2**.

The evolution of the electronic absorption spectra of the optically pure asymmetric complex (–)-**4** in $CHCl_3$/MeOH mixtures was very similar to that observed for the C_3-symmetric homologue **1** (Figure S93): Slight hypsochromic shift of the main absorption band, 39% decrease of its optical density,

broadening and rise of an absorption tail around 320 - 330 nm. Monitoring the intensity of this absorption against the solvent composition showed that it started to increase significantly for ≥ 80% MeOH. The evolution of the emission spectra in aerobic conditions upon excitation at 330 nm (Figure S94) was reminiscent of that observed in the case of **1**, except that upon addition of MeOH the emission at 393 nm gradually predominated over the one at 375 nm, which changed to a shoulder, and decreased only for ≥ 30% MeOH. The different intensity ratios I_{538}^{99}/I_{390}^{0}, $I_{538}^{99}/I_{393}^{99}$, and I_{535}^{0}/I_{390}^{0} were 0.52, 3.58, and 0.040, respectively. The final I_{538}/I_{393} ratio remained < 1, as for **2**, whereas in the case of **1**, the corresponding intensity ratio was > 1.

The behaviors of the enantiomers of **1** in the $CHCl_3$/MeOH mixtures were examined by emission spectroscopy and ECD. The evolution of the emission spectra of (–)-**1** are reproduced in Figure S95. As for the racemate, upon addition of increasing MeOH proportion the emission at 377 nm decreased, while the new emission band at low energy appeared clearly for 60% MeOH at 545 nm. It grew up abruptly between 70 and 80 % MeOH, while its maximum was shifted to 537 nm. The different intensity ratios I_{537}^{99}/I_{379}^{0}, I_{537}^{99}/I_{379}^{0}, and I_{537}^{0}/I_{377}^{0} were 1.26, 6.39, and 0.041, respectively. Similar observations were done in the case of (+)-**1** (Figure S96), the intensity ratios I_{536}^{99}/I_{385}^{0}, $I_{536}^{99}/I_{385}^{99}$, and I_{536}^{0}/I_{385}^{0} being respectively 1.51, 11.2, and 0.046. Plots of the emission intensities at ca 540 nm for (–)-**1** and (+)-**1** as a function of the MeOH/$CHCl_3$ ratio are shown in Figure S97.

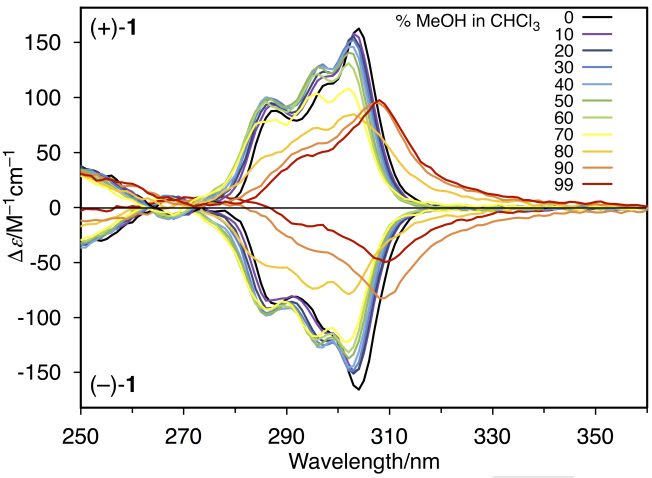

Figure 8. Evolutions of the ECD spectra of 10^{-5} solutions of the enantiomers of complex **1** in in $CHCl_3$/MeOH mixtures at room temperature.

The ECD spectra of the optically active versions of **1** (Figures 8, and S98-S99) showed approximatively mirror-image evolutions in $CHCl_3$/MeOH, which were reminiscent of the changes observed in the absorption spectra of the racemate. For example, in the case of (+)-**1**, the main absorption at 304 nm decreased in intensity and was progressively shifted to shorter wavelength (302 nm) until the MeOH content was < 80%. Considerable band broadening was already apparent at this latter concentration, but at 90% MeOH secondary maxima had completely disappeared and the main maximum had shifted to longer wavelength (308 nm). Noteworthy also was the fact that the low energy band of the B_{1u} couplet (negatively signed for (+)-**1**, positively signed for (–)-**1**) disappeared at MeOH/$CHCl_3$ ≥ 80:20, v/v. Reports on optically-active organic molecular spherical nanoparticles are rare.[90] Calculations, in the frame of the Mie theory, of the ECD spectra of hypothetical solutions of spherical nanoparticles of optically-active poly-*L*-glutamic acid (PGA) were reported, and compared to the experimental ECD spectrum of a PGA solution.[91] This study had shown that, as the radius of the spheres increased from 30 to 100 nm, the peak maxima and the cross-over points of the bisignate signal of the PGA solution observed experimentally shifted bathochromically, while the overall shape of the ECD signal was increasingly distorted.

Emission in the solid state. The emission of powdered/ground samples of the complexes **1** - **3** was recorded (Figure S100). Upon irradiation of the solid samples at the excitation wavelength used for the irradiation for their solutions in $CHCl_3$/MeOH mixtures (330 nm), a blue-green luminescence was observed, with maxima at 520, 500, and 486 nm for **1**, **2**, and **3**, respectively. Remarkably, the shape of the emission band of **3** together with its maximum at 486 nm and shoulder at 514 nm were reminiscent of the characteristics of the emission band observed for the same complex in the 1:99 $CHCl_3$/MeOH mixture (Figures 7b and S101). However, the maxima of the solid state emissions of complexes **1** and **2** were shifted to higher energies by comparison with the maxima recorded in 1:99 $CHCl_3$/MeOH (respectively 540 and 550 nm).

Dynamic light scattering. Solutions of **1** at the concentration used for the electronic absorption and emission studies (10^{-5} M) were examined by dynamic light scattering (DLS). The selected MeOH/$CHCl_3$ ratios were 20:80, 50:50, 80:20 and 99:1, v/v. These experiments showed that the solutions contained nanoparticles, the size of which depended on the MeOH/$CHCl_3$ ratios. The corresponding distribution diagrams are shown in Figure S102. Whereas the 20:80 composition did not show any nanoparticle, nanoparticles were detected for the 50:50 ratio. The distribution diagram showed that the size of the nanoparticles ranged between 25 and *ca* 80 nm, with a maximum of population for sizes of 30 - 35 nm. A similar distribution was observed in the case of the 80:20 composition, except that the proportion of nanoparticles ranging from 35 to 40 nm was higher than in the case of the 50:50 composition. Finally, the 99:1 composition contained a broader distribution of nanoparticles, with sizes ranging from 50 to 200 nm, the maximum of population concerning sizes centered around 80 nm.

Interpretation of the results. Electronic spectroscopy studies of the complexes **1** - **3** in $CHCl_3$/MeOH mixtures and, in the case of complex **1**, complementary DLS experiments, demonstrated that the complexes formed aggregates at MeOH ratios > 40%, v/v. In addition, the variations of the absorbance and emission intensities at fixed wavelengths indicated that the progression of the aggregation was not linear: It increased more rapidly for MeOH ratios > 60%, v/v. As aggregate formation does not occur in $CHCl_3$/MeCN, even at high MeCN content, it is likely that it results from solvophobic interactions. The CTB complexes being highly lipophilic, they form compacted supramolecular assemblies in order to minimize their exposition to methanol. As a consequence of the proximity of the chromophores, strong

hypochromic shifts of the absorption[38] and differential absorption (in the case of the optically-active complexes), are observed. The most interesting electronic consequence of the aggregation is the development of a green emission ($\lambda_{em} \approx 540$ - 550 nm). Aggregation-induced emission of gold(I) acetylides was observed in several cases, in particular in water,[33] water/solvent mixtures,[15,25] and in mixed organic solvent systems,[33] in the form of a low energy band at wavelengths ranging from 550 to 650 nm. In the solid state, strong bathochromic shifts (e.g. from 420 to 550 nm) of the solution room temperature triplet emission of dinuclear complexes whose X-ray diffraction analysis gave Au···Au distances around 3.136 - 3.153 Å, have been noted.[2,5] In other cases, the red shift was clearly the consequence of favorable π-π stacking interactions.[5] We note that such a low energy emission was also observed in multinuclear gold(I) acetylide complexes in which the gold atoms could be brought closer together by an external stimulus, such as the complexation of cations.[25,26,33] The red-shifted emission was assigned as arising from a d_σ*–p_σ excited state.[5] We tentatively assign the green emission observed for solutions of complexes **1** and **2** in $CHCl_3$/MeOH mixtures of compositions ranging between 50:50 and 1:99 to aggregation-induced Au···Au interactions. In the case of **1**, upon increasing the MeOH content, this emission is shifted hypochromically and hypsochromically from its initial intensity and wavelength values at the maximum, respectively. The blue shift indicates that other interactions than aurophilic interactions contribute to the emission changes. The case of complex **3** is particular, as, contrary to **1** and **2**, it shows a weak emission between 500 and 600 nm for < 99% MeOH ratios, and a sudden change of the shape of the emission band above 450 nm for MeOH/$CHCl_3$ 99:1. In addition, this new emission band shows the same features as the emission band collected in the solid state.

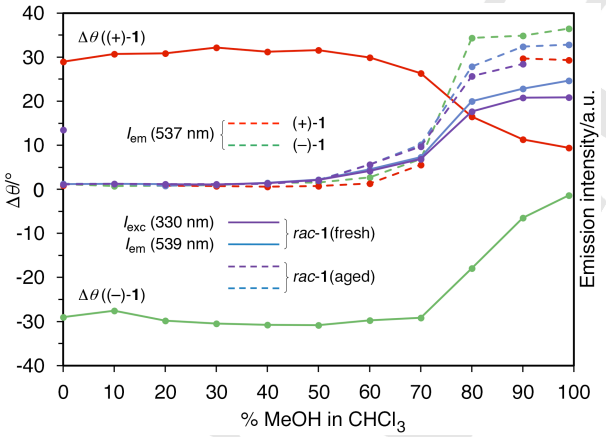

Figure 9. (Left) ellipticity of 10^{-5} M solutions of (+)-**1** and (–)-**1** and (right) emission intensities of 10^{-5} M solutions of (+)-**1** and (–)-**1** and their racemic mixtures (freshly prepared and aged solutions) as a function of the MeOH content in $CHCl_3$/MeOH solvent mixtures. Significant differences between the evolution of the emission intensities of the optically pure compounds, on the one hand, and the racemic mixtures, on the other hand, were observed in the region between 40 and 70% MeOH in $CHCl_3$.

A unique property of compounds **1** - **3** among existing gold(I) acetylide complexes is their chirality, if we except the case of $[Fe(bipy)_3]^{2+}$ conjugates.[31] We have studied the electronic spectroscopy properties of the aggregates of **1** formed from the racemate (±)-**1**, and the optically-active forms (+)-**1** and (–)-**1**. Whereas the aggregates made from the latter forms are homochiral, we may wonder about the enantiomeric composition of the aggregates made from (±)-**1**, as they can be heterochiral or homochiral. If the aggregates are homochiral, they can be considered as precursors of conglomerates. As shown in Figure 9, the variations of the emission intensities of the band at ~ 539 nm of (+)-**1** and (–)-**1** in $CHCl_3$/MeOH mixtures are comparable with each other, with an onset at 60% MeOH (see also Figure S97), whereas in the case of the racemate, this emission is clearly detectable at lower methanol contents (*i.e.* between 40 and 50%). This means that the composition of the aggregates made from *rac*-**1** differs qualitatively from the compositions of the aggregates made from the optically pure complexes: Whereas the latter are necessarily homochiral, the former are probably heterochiral, which makes these assemblies true racemates.

Conclusion

Three chiral trinuclear phosphine gold(I) alkynyl complexes derived from cyclotribenzylene have been synthesized and characterized. The complexes were found mainly in monomeric forms, as suggested by ^{1}H NMR spectroscopy, diffusion-ordered spectroscopy, and electrospray ionisation mass spectrometry studies, ruling out the formation of molecular cages by aurophilic interactions. The enantiomers of the ligand precursor as well as those of the triphenylphosphine complex have been separated by chiral HPLC. As arylacetylide gold(I) complexes of the literature, the complexes showed long-lived (30 μs) phosphorescence in chlorinated solvents; in addition, we could observe weak fluorescence in aerated solutions. We also investigated the luminescence properties of the complexes as solutions in $CHCl_3$/MeOH mixtures and as solids, and found that when the methanol content exceeded 50%, a green emission band centered around 540 nm developed at the expense of the UV fluorescence. As shown by associated changes in the absorption spectra and, for the triphenylphosphine complex, in the electronic circular dichroism spectra, this luminescence switch is due to the formation of aggregates, which were investigated by dynamic light scattering. Aggregate formation originates from the solvophobic response of the complexes in the presence of methanol. The aggregation-induced emission (AIE) observed is likely to arise from electronic excited states involving contributions from Au···Au bonds, due to the constrained proximity of the complexes in the aggregates. In this contribution, we have examined the AIE of enantiomerically pure gold(I) acetylides, which allowed us to show that the aggregates obtained from the racemic form of the complex are racemates. Future directions of this work will concern investigations on the possibility to observe circularly polarized luminescence from the optically active aggregates.

Experimental Section

Materials, methods, and instrumentation. The following abbreviations were used: THF (tetrahydrofuran) and DMF (*N*,*N*-dimethylformamide). Unless otherwise stated, all reactions were performed under argon using the following solvents and liquid reagents, which were dried and distilled under argon: DMF (anhydrous magnesium sulfate), THF

(Na/benzophenone), dichloromethane (P_2O_5), methanol (Mg), triethylamine (KOH), and acetone (K_2CO_3). Chloroform and methanol used for electronic spectroscopy were redistilled. Other commercially available solvents and reagents were used as received. Separations by flash column chromatography used either silicagel (Si 60, 40-63 μm, from VWR, or Geduran, from Merck) or aluminum oxide 90 (standardized, according to Brockmann, from Merck). CTB(H,OTf)[56], [Au(PPh_3)Cl],[92] and [Au(SMe_2)Cl][92] were synthesized according to the literature. NMR spectra were recorded on Bruker Avance III 400 MHz, 500 MHz and 600 MHz spectrometers. Chemical shifts were reported using the residual solvent ^{1}H signal (7.26 and 77.16 ppm for $CHCl_3$) as internal reference for ^{1}H NMR and ^{13}C NMR, respectively, and the phosphorus signal (set at 0 ppm) of H_3PO_4 placed inside an insert for ^{31}P NMR. IR spectra were recorded using a Bruker Alpha II spectrophotometer. Electronic absorption spectra were recorded using a Cary 5000 double beam spectrophotometer from Agilent technologies and electronic emission spectra were recorded using a JASCO 8300 spectrofluorimeter. Emission lifetimes were measured with a Horiba Jobin-Yvon Fluorolog FL3-22 spectrofluorimeter equipped with a 340 nm NanoLed (fluorescence) and a xenon lamp delivering 3 μs pulses (phosphorescence). Solutions for experiments in oxygen-free conditions were degassed by freeze-pump-thaw cycles in Schlenk flasks and transferred via cannula into quartz cells equipped with a septum. Mass data were obtained using a MicrOTOF-QII (Bruker Daltonics, Bremen, Germany) mass spectrometer fitted with Z-spray electrospray ion source and with a mass range of 2 - 4000 Thomson. Dynamic light scattering experiments were performed by using a Malvern Zetasizer NanoZS apparatus. STEM experiments were carried out using a Quanta250 FEG apparatus from Thermofischer. ECD spectra and the associated electronic absorption spectra were measured on a JASCO J-815 spectrometer equipped with a JASCO Peltier cell holder PTC-423 to maintain the temperature at 25.0 ± 0.2°C. A cell of 1 mm of optical pathlength was used. The CD spectrometer was purged with nitrogen before recording each spectrum, which was baseline subtracted. The baseline was always measured for the same solvent and in the same cell as the samples. The spectra were presented without smoothing and further data processing. Optical rotations were measured on a JASCO P-2000 polarimeter with a halogen lamp (589, 578, 546, and 436 nm) in a 10 cm cell thermostated at 25 °C with a Peltier controlled cell holder. Electronic circular dichroism studies of the optically-pure gold CTBs in $CHCl_3$/MeOH solutions was performed using a JASCO J-810 spectrometer equipped with a Peltier PTC-423S/L temperature controller from JASCO. **CAUTION**: Some gold acetylide were found to be shock sensitive. These compounds should be handled in small quantities using protective equipment.

CTB(H,C_2TMS). CTB(H,OTf) (0.373 g, 0.522 mmol) and [Pd(PPh_3)$_2$$Cl_2$] (0.0767 g, 0.109 mmol, 20 mol%) were dissolved in DMF (20 mL). Trimethylsilylacetylene (0.664 mL, 4.70 mmol, 9 equiv) and triethylamine (3.5 mL, 25 mmol) were added, and the reaction mixture heated at 70 °C overnight. The reaction mixture was cooled to room temperature. The solvent was removed under vacuum, leaving a dark brown residue, which was purified by column chromatography using either silicagel and cyclohexane/dichloromethane 7:2 as eluent, or aluminum oxide and heptane/toluene 4:1 as eluent. CTB(H,C_2TMS) was obtained as a yellow solid (0.279 g, 96% yield). It can be recrystallized from CH_2Cl_2/MeOH, m.p. 220-222 °C; ^{1}H NMR (400 MHz, $CDCl_3$, 298 K): δ = 7.429 (d, $^4J_{H,H}$ = 1.6 Hz, 3 H; α'-H), 7.322 (d, 3 H, $^3J_{H,H}$ = 8.0 Hz, α-H), 7.222 (dd, $^3J_{H,H}$ = 8.0 Hz and $^4J_{H,H}$ = 1.6 Hz, 3 H; γ-H), 4.773 (d, $^2J_{H,H}$ = 13.6 Hz, 3 H; a-H), 3.676 (d, $^2J_{H,H}$ = 13.6 Hz, 3 H; e-H), 0.234 (s, 27 H; SiCH_3) ppm; ^{1}H NMR (600.23 MHz, d^6-acetone, 300 K) δ = 7.602 (d, $^4J_{H,H}$ = 1.8 Hz, 3 H; α'-H), 7.544 (d, $^3J_{H,H}$ = 8.1 Hz, 3 H; α-H), 7.232 (dd, $^3J_{H,H}$ = 8.1 Hz, $^4J_{H,H}$ = 1.8 Hz, 3 H; γ-H), 5.013 (d, $^2J_{H,H}$ = 13.5 Hz, 3 H; a-H), 3.843 (d, $^2J_{H,H}$ = 13.5 Hz, 3 H; e-H), 0.204 (s, 27 H; SiCH_3) ppm; ^{13}C{^{1}H} NMR (150.94 MHz, d^6-acetone, 300 K) δ = 141.46 (s; β-C), 140.72 (s; β'-C or γ'-C), 134.27 (s; α'-C), 131.44, 131.32 (2 s; α-C and γ-C), 122.65 (s; β'-C or γ'-C), 105.93 (s; δ'-C), 94.08 (s; ε'-C), 36.86 (s; CH_2), 0.04 (s; SiCH_3) ppm; IR: $\tilde{\nu}$ = 2959 (w), 2152 (m), 1493 (m), 1479 (m), 1247 (m), 960 (m), 889 (m), 835 (s), 803 (sh, m), 749 (m), 718 (w), 698 (w), 649 (m), 627 (m), 590 (w), 529 (w) cm^{-1}; HR-MS (Electrospray ionization time-of-flight): m/z calcd for $C_{36}H_{43}Si_3$, 559.26726, found 559.26525 ([M+H]$^+$), calcd for $C_{36}H_{42}Si_3K$, 597.22314, found 597.22062 ([M+K]$^+$); elemental analysis: calcd for $C_{36}H_{42}Si_3$·2/3H_2O, C 75.73, H 7.65, found, C 75.63, H 7.59.

CTB(H,C_2H). CTB(H,C_2TMS) (0.197 g, 0.358 mmol) was dissolved in THF (10 mL). Tetrabutylammonium fluoride (4.0 mL of a 1 M solution in THF, 4.0 mmol) was added, and the solution was allowed to react at room temperature overnight. The solvent was evaporated under vacuum, and the residue stirred in dichloromethane (40 mL) and water (50 mL). The aqueous phase was further extracted twice with dichloromethane (80 mL). The combined organic phases were washed with water, dried with anhydrous magnesium sulfate, and concentrated by rotary evaporation to give a yellow-brown solid, which was purified by column chromatography on silica gel, using cyclohexane/dichloromethane 7:2 as eluent, to afford CTB(H,C_2H) as a yellowish powder (0.100 g, 83% yield). M.p. > 220 °C (dec); ^{1}H NMR (400 MHz, $CDCl_3$, 298 K): δ = 7.484 (d, $^4J_{H,H}$ = 1.6 Hz, 3 H; α'-H), 7.338 (d, $^3J_{H,H}$ = 8.0 Hz, 3 H; α-H), 7.248 (dd, $^3J_{H,H}$ = 8.0 Hz, $^4J_{H,H}$ = 1.6 Hz, 3 H; γ-H), 4.815 (d, $^2J_{H,H}$ = 13.6 Hz, 3 H; a-H), 3.717 (d, $^2J_{H,H}$ = 13.6 Hz, 3 H; e-H), 3.020 (s, 3 H; C_2H) ppm; ^{1}H NMR (600.23 MHz, d^6-acetone, 300 K): δ = 7.646 (d, $^4J_{H,H}$ = 1.8 Hz, 3 H; α'-H), 7.577 (d, $^3J_{H,H}$ = 8.1 Hz, 3 H; α-H), 7.251 (dd, $^3J_{H,H}$ = 8.1 Hz, $^4J_{H,H}$ = 1.8 Hz, 3 H; γ-H), 5.031 (d, $^2J_{H,H}$ = 13.5 Hz, 3 H; a-H), 3.851 (d, $^2J_{H,H}$ = 13.5 Hz, 3 H; e-H), 3.563 (s, 3 H; C_2H) ppm; ^{13}C{^{1}H} NMR (150.94 MHz, d^6-acetone, 300 K): δ = 141.48 (s; β-C), 140.74 (s; β'-C or γ'-C), 134.54 (s; α'-C), 131.45 (s; α-C), 131.35 (s; γ-C), 121.89 (s; β'-C or γ'-C), 84.05 (s; δ'-C), 78.87 (s; ε'-C), 36.80 (s; CH_2) ppm; ^{13}C{^{1}H} NMR (125 MHz, $CDCl_3$, 298 K): δ = 140.0 (s, β-C), 139.1 (s, β'-C), 133.9 (s, α'-C), 131.1 (s, γ-C), 130.4 (s, α-C), 121.1 (s, γ'-C), 83.5 (s, C_2H), 36.9 (CH_2) ppm. IR: $\tilde{\nu}$ = 3271 (m), 2918 (w), 2099 (br, w), 1561 (w), 1491 (m), 1474 (m), 1399 (w), 1251 (br, w), 1161 (w), 1091 (w), 944 (w), 892 (m), 828 (m), 803 (w), 754 (m), 692 (m), 676 (m), 648 (sh, m), 621 (s), 585 (s), 550 (m), 533 (m), 505 (m), 431 (m), 405 (m); HR-MS (Electrospray ionization time-of-flight): m/z calcd for $C_{27}H_{19}$ 343.14868, found 343.14689 ([M+H]$^+$); elemental analysis: calcd for $C_{27}H_{18}$·2/3H_2O, C 91.49, H 5.50, found, C 91.48, H 5.41.

[CTB(H,C_2Au)]n. A solution of sodium acetate (0.0753 g, 0.918 mmol) in a mixture of THF (0.5 mL) and methanol (3 mL) was added to a solution of CTB(H,C_2H) (0.0349 g, 0.102 mmol) and [AuCl(SMe_2)] (0.090 g, 0.306 mmol, 3 equiv) in a mixture of THF (12 mL) and methanol (3 mL). The resulting reaction mixture was stirred overnight at room temperature to produce a black green precipitate. The solid was collected by filtration, washed with THF, methanol, water, methanol again, and finally diethyl ether, after which it was dried. This reagent, which is poorly soluble, was used without further purification.

CTB(H,C_2AuPPh_3) (**1**). Method A: CTB(H,C_2H) (0.01 g, 0.0292 mmol), [Au(PPh_3)Cl] (0.058 g, 0.117 mmol), and sodium methoxide (0.024 g, 0.438 mmol) were mixed in methanol/THF (1:1, v/v, 10 mL) at 40 °C. After stirring of the reaction mixture for 3 days, the solvents were removed by rotary evaporation. The residue was taken into dichloromethane, then filtered to remove the excess of sodium methoxide, and sodium chloride, which afforded a clear yellow solution. The latter was concentrated to a volume of about 1 mL, and treated by dropwise addition of cyclohexane (1.5 mL) until precipitation of the product occurred. The precipitate was stored at 0 °C overnight, filtered, and dried under vacuum, affording a yellow powder of complex **1**. Yield: 0.030 g, 60%. Method B: A solution of triphenylphosphine (0.0321 g, 0.122 mmol) in THF (1.5 mL) was added to a suspension of [CTB(H,C_2Au)]$_n$ (0.038 g, 0.041 mmol) in dichloromethane (4 mL) and the reaction mixture stirred overnight. It was subsequently filtered by using a sintered glass funnel of porosity 4 to give a clear light yellow solution, which was evaporated to dryness. The residue was washed with methanol, affording complex **1** as a light yellow crystalline solid. Yield: 0.055 g, 78%. ^{1}H NMR (500.13 MHz, $CDCl_3$, 295 K): δ = 7.553 (d, $^3J_{H,H}$ = 7.7 Hz, $^4J_{H,H}$ = 1.3 Hz, 9 H; o-H), 7.527 (dd, $^3J_{H,H}$ = 7.7 Hz, $^4J_{H,H}$ = 1.3 Hz, 9 H; o'-H), 7.510 (d, $^4J_{H,H}$ = 1.5 Hz, 3 H; α'-H), 7.477 (d, $^3J_{H,H}$ = 6.5 Hz, 9 H; p-H), 7.432 (2 d, $^3J_{H,H}$ = 6.50 Hz, 18 H; m-H, m'-H), 7.258 (d, $^3J_{H,H}$ = 8.0 Hz, 3 H; α-H), 7.206 (dd, $^3J_{H,H}$

= 8.0 Hz, $^4J_{H,H}$ = 1.0 Hz, 3 H; γ-H), 4.746 (d, $^2J_{H,H}$ = 13.3 Hz, 3 H; a-H), 3.629 (d, $^2J_{H,H}$ = 13.3 Hz, 3 H; e-H) ppm; $^{13}C\{^1H\}$ NMR (125.76 MHz, $CDCl_3$, 295 K): δ = 138.81 (s; β'-C), 138.16 (s; β-C), 134.46 (d, $^3J_{C,P}$ = 13.8 Hz; o-C, o'-C), 134.16 (s; α'-C), 131.62 (d, $^4J_{C,P}$ = 1.3 Hz; p-C), 131.02 (s; γ-C), 130.27 (s; α-C), 129.94 (d, $^1J_{C,P}$ = 56.6 Hz; i-C), 129.23 (d, $^3J_{C,P}$ = 11.3 Hz; m-C, m'-C), 123.37 (s; γ'-C), 104.51, 104.29 (2 s; δ'-C, ε'-C), 37.07 (s; CH_2) ppm; $^{31}P\{^1H\}$ NMR (161.98 MHz, $CDCl_3$, 298 K) δ = 42.97 ppm. IR (KBr): $\tilde{\nu}$ = 3051, 3016, 2918, 2851, 2098 (C≡C), 1962, 1893 (br, vw), 1600 (w), 1490, 1478 (m), 1436 (s), 1385, 1309, 1182, 1159 (w), 1100 (s), 1027, 998, 890, 833 (w), 745, 708 (m), 693, 537 (s), 509 (m) cm^{-1}; HR-MS (Electrospray ionization time-of-flight): m/z calcd for $C_{81}H_{61}Au_3P_3$ ($[M+H]^+$) 1717.29827, found 1717.299 (6830NZ - 15 eV) ; elemental analysis: calcd for $C_{81}H_{60}Au_3P_3{\cdot}2CH_2Cl_2$, C 52.83, H 3.42, found, C 52.47, H 3.46.

CTB(H,C_2AuPEt$_3$) (2). CTB(H,C_2H) (0.02 g, 0.0585 mmol), [Au(PEt_3)Cl] (0.063 g, 0.181 mmol), and sodium methoxide (0.047 g, 0.877 mmol) were mixed in methanol/THF (1:1, v/v, 16 mL) at 40 °C. After stirring of the reaction mixture for 4 days, the solvents were removed by rotary evaporation. The residue was taken into dichloromethane, then filtered to remove the excess of sodium methoxide, and sodium chloride, affording a clear yellow solution. The latter was concentrated and treated by dropwise addition of cyclohexane until precipitation of the product occurred. The precipitate was stored at 0 °C overnight, filtered, and dried under vacuum, affording a yellow powder of complex **2**. Yield: 0.050 g, 68%. ^{1}H NMR (500.13 MHz, $CDCl_3$, 295 K): δ = 7.459 (d, $^4J_{H,H}$ = 1.5 Hz, 3 H; α'-H), 7.215 (d, $^3J_{H,H}$ = 8.0 Hz, 3 H; α-H), 7.163 (dd, $^3J_{H,H}$ = 8.0 Hz, $^4J_{H,H}$ = 1.5 Hz, 3 H; γ-H), 4.715 (d, $^2J_{H,H}$ = 13.5 Hz, 3 H; a-H), 3.595 (d, $^2J_{H,H}$ = 13.5 Hz, 3 H; e-H), 1.774 (quint, $^3J_{H,H}$ = $^3J_{H,P}$ = 7.8 Hz, 18 H; PCH_2), 1.176 (td, $^3J_{H,H}$ = 7.8 Hz, $^3J_{H,P}$ = 18.0 Hz, PCH_2CH_3) ppm; $^{13}C\{^1H\}$ NMR (125.76 MHz, $CDCl_3$, 295 K): δ = 138.77 (β'-C), 130.01 (β-C), 134.09 (α'-C), 130.94 (γ-C), 130.19 (α-C), 123.51 (γ'-C), 104.6 (2 s, δ'-C and ε'-C), 37.03 (CH_2), 17.92 (d, $^1J_{C,P}$ = 32.7 Hz; PCH_2), 8.97 (PCH_2CH_3) ppm; $^{31}P\{^1H\}$ NMR (161.98 MHz, $CDCl_3$, 298 K) δ = 37.22 ppm; IR (KBr): $\tilde{\nu}$ = 3303, 3239 (vw), 3060, 3017 (w), 2965 (vs), 2930 (s), 2874 (m), 2738, 2427 (vw), 2102 (w; C≡C), 1901 (br, vw), 1601 (m), 1557 (w), 1492 (s), 1479, 1454, 1415, 1381 (m), 1261 (s), 1233, 1220 (m), 1093 (br, s), 1039 (br, vs), 952 (w), 892 (m), 865 (w), 802 (s), 772 (vs), 707 (w), 665 (m), 634 (m), 590, 571, 532, 515, 441 (w) cm^{-1}; HR-MS (Electrospray ionization time-of-flight): m/z calcd for $C_{45}H_{63}Au_3P_3$ ($[M+H]^+$) 1285.29827, found 1285.29; elemental analysis: calcd for $C_{45}H_{61}Au_3P_3{\cdot}4/3C_6H_{12}$, C 45.57, H 5.48, found, C 45.61, H 5.43.

CTB(H,C_2AuPCy$_3$) (3). CTB(H,C_2H) (0.008 g, 0.0234 mmol), [Au(PCy_3)Cl] (0.042 g, 0.082 mmol), and sodium methoxide (0.019 g, 0.351 mmol) were mixed in methanol/THF (1:1, v/v, 10 mL) at 40 °C. After stirring of the reaction mixture for 1 day, the solvents were removed by rotary evaporation. The residue was taken into dichloromethane, then filtered to remove the excess of sodium methoxide, and sodium chloride, which afforded a clear yellow solution. The latter was concentrated to a volume of about 1 mL, and treated by dropwise addition of MeOH (1.5 mL) until precipitation of the product occurred. The precipitate was stored at 0 °C overnight, filtered, and dried under vacuum, affording complex **3** as a yellow powder. Yield: 0.030 g, 72%. ^{1}H NMR (500.13 MHz, $CDCl_3$, 295 K): δ = 7.473 (d, $^3J_{H,H}$ = 1.0 Hz, 3 H; α'-H), 7.195 (AB, $^3J_{AB}$ = 8.0 Hz, $\Delta\nu$ = 11.2 Hz, $^4J_{H,H}$ = 1.5 Hz, 6 H; α-H, γ-H), 4.704 (d, $^2J_{H,H}$ = 13.0 Hz, 3 H; a-H), 3.584 (d, $^2J_{H,H}$ = 13.0 Hz, 3 H; e-H), 1.982 (m, 27 H; 1-H, 3,3'-H), 1.840 (br s, 18 H; 2,2'-H), 1.716 (br s, 9 H; 4-H), 1.466 (br s, 18 H; 3,3'-H), 1.257 (br m, 27 H; 4 H, 2,2'-H) ppm; $^{13}C\{^1H\}$ NMR (125.77 MHz, $CDCl_3$, 295 K): δ = 138.69 (s; β'-C), 137.89 (s; β-C), 134.15 (α'-C), 130.95 (s; γ-C), 130.21 (s; α-C), 123.58 (s; γ'-C), 103.92 (s; ε'-C), 103.74 (s; δ'-C), 37.09 (s; CH_2), 33.28 (d, $^1J_{CP}$ = 27.8 Hz; 1-C), 30.79 (s; 3,3'-C), 27.28 (d, $^2J_{CP}$ = 11.7 Hz; 2,2'-C), 26.03 (s; 4-C) ppm; $^{31}P\{^1H\}$ NMR (121.49 MHz, $CDCl_3$, 298 K) δ = 56.77 ppm; IR (KBr): $\tilde{\nu}$ = 2926 (s; C–H), 2851 (m), 2108 (vw; C≡C), 1492 (w), 1446 (m), 1218, 1177, 1113, 1004, 881, 853 (w), 755 (s), 664, 633 (w), 519 (m); HR-MS (Electrospray ionization time-of-flight): m/z calcd for $C_{81}H_{115}Au_3P_3$ ($[M+H]^+$) 1771.72082, found 1771.720; elemental analysis: calcd for $C_{81}H_{114}Au_3P_3{\cdot}2CH_2Cl_2$, C 51.35, H 6.13, found, C 51.41, H 6.18.

Separation of the enantiomers of CTB(H,C_2H). CTB(H,C_2H) (*ca* 0.049 g) was dissolved in CH_2Cl_2 (20 mL) and injected 400 times in 50 μL portions, each every 3 min, into a Chiralpak IB column (250 × 10 mm). Elution was performed using hexane/ethanol/dichloromethane (70:10:20) as mobile phase at a flow-rate of 5 mL min^{-1} and detection by absorbance in the UV at 254 nm. The fractions collected were kept in an ice bath. The first fraction contained (–)-CTB(H,C_2H) (0.012 g; > 99.5 ee). The second one, collected between 6.4 and 7.1 minutes afforded (+)-CTB(H,C_2H) (0.014 g; > 99 ee).

Separation of the enantiomers of complexes 1 and 4. Complex **1** (0.046 g) was dissolved in CH_2Cl_2 (1.5 mL) and injected 37 times in 40 μL portions, each every 8 min, into a Chiralpak IF column (250 × 4.6 mm). Elution was performed using hexane/ethanol/dichloromethane (20:40:40) as mobile phase at a flow-rate of 1 mL min^{-1} and detection by UV absorbance at 254 nm. Three fractions were obtained. The first fraction (0.0204 g) was subjected to a second HPLC purification (see below). The second fraction contained (+)-**4** (0.0020 g; 93% purity). The third fraction contained (+)-**1** (0.0124 g; 94% purity). The first fraction issued from the Chiralpak IF column was dissolved in CH_2Cl_2 (0.75 mL) and injected 22 times in 30 μL portions, each every 10 min, into a (*S*,*S*)-Whelk-O1 column (250 × 4.6 mm), eluting using hexane/ethanol/dichloromethane 40:30:30 as mobile phase and detection by UV absorbance at 254 nm. This process afforded a first fraction containing (–)-**4** (0.0028 g; 100% purity), and a second fraction containing (–)-**1** (0.0096 g, 98.4% purity).

CTB(3H;2C_2AuPPh$_3$,C_2H) (4). HR-MS (ESI): m/z calcd for $C_{63}H_{47}Au_2P_2$ ($[M+H]^+$) 1259.950, found 1259.245. Its ^{1}H NMR and ^{13}C spectra are shown in the Supporting Information.

Kinetics of racemisation of (+)-CTB(H,C_2H). An enantioenriched sample of (+)-CTB(H,C_2H) (~ 0.3 mg) was heated in dichloromethane (~ 25 mL) at 40 °C. Aliquots (10 μL) were withdrawn and injected into a Chiralpak IB HPLC column (250 × 4.6 mm). Elution using heptane/ethanol/dichloromethane 70:10:20 as mobile phase at a flow-rate of 1 mL min^{-1} and detection by UV absorbance at 254 nm of 1 mL/min afforded a chromatogram from which the percentage of the (+)-CTB(H,C_2H) enantiomer at a given time was determined.

Mass spectrometry experiments. Each sample at 10^{-4} mol L^{-1} in $CHCl_3$ was diluted to a final concentration of 5×10^{-5} mol L^{-1} with an equal volume of isopropanol containing 1% v/v of formic acid prior to injection into the mass spectrometer. The mass spectrometer was operated in the positive ion mode, with a potential of 3500 V applied to the electrospray probe body and the source temperature set to 180 °C. Mass spectrometry data were acquired from m/z = 300 to 3000. The ISCID energy was kept at 0 eV, while the energy of the collision cell (E_{coll}) was varied from 2 to 20 eV in order to observe the dissociation of potential dimers. The mass calibration was performed using a mix of Tune Low (Agilent Technologies G1969-8500) prior to analysis. The data were processed with the Data Analysis software from Bruker Daltonics.

Acknowledgements

We thank the French National Research Agency (ANR) through the "Programme d'Investissement d'Avenir" under contract 17-EURE-0016 (PhD fellowship to JZ), the Embassy of France in Germany (post-doctoral fellowship to AS), the CNRS, the University of Strasbourg, and the University Bourgogne Franche-Comté for financial support. Dr. Martine Heinrich, Dr. Mélanie Legros, and Mr. Thomas Weissenberger are warmly thanked for their help in the use of the fluorescence spectroscopy instruments, the DLS particle size analyzer, and the IR spectrophotometer, and Noémie Schneider for the

elemental analyses. The referees are thanked for their helpful comments.

Keywords: Alkyne ligands • Gold • Chirality • Luminescence • Aggregation

[1] G. Calvin, G. E. Coates, P. S. Dixon, *Chem. Ind. (London)* **1959**, 1628.
[2] D. Li, X. Hong, C.-M. Che, W.-C. Lo, S.-M. Peng, *J. Chem. Soc. Dalton Trans.* **1993**, 2929-2932.
[3] T. E. Müller, S. W.-K. Choi, D. M. P. Mingos, D. Murphy, D. J. Williams, V. W.-W. Yam, *J. Organomet. Chem.* **1994**, *484*, 209-224.
[4] V. W.-W. Yam, S. W.-K. Choi, *J. Chem. Soc. Dalton Trans.* **1996**, 4227-4232.
[5] M. J. Irwin, J. J. Vittal, R. J. Puddephatt, *Organometallics* **1997**, *16*, 3541-3547.
[6] H.-Y. Chao, W. Lu, Y. Li, M. C. W. Chan, C.-M. Che, K.-K. Cheung, N. Zhu, *J. Am. Chem. Soc.* **2002**, *124*, 14696-14706.
[7] V. W.-W. Yam, K.-L. Cheung, S.-K. Yip, K.-K. Cheung, *J. Organomet. Chem.* **2003**, *681*, 196-209.
[8] H.-S. Lo, N. Zhu, V. K.-M. Au, V. W.-W. Yam, *Polyhedron* **2014**, *83*, 178-184.
[9] W.-Y. Wong, S.-Y. Poon, *J. Inorg. Organomet. Polym.* **2008**, *18*, 155-162.
[10] W.-Y. Wong, Y. Guo, C.-L. Ho, *J. Inorg. Organomet. Polym.* **2009**, *19*, 46-54.
[11] S.-Y. Poon, W.-Y. Wong, K.-W. Cheah, J.-X. Shi, *Chem. Eur. J.* **2006**, *12*, 2550-2563.
[12] Y. Lin, J. Yin, J. Yuan, M. Hu, Z. Li, G.-A. Yu, S. H. Liu, *Organometallics* **2010**, *29*, 2808-2814.
[13] Y.-C. Chang, K.-C. Tang, H.-A. Pan, S.-H. Liu, I. O. Koshevoy, A. J. Karttunen, W.-Y. Hung, M.-H. Cheng, P.-T. Chou, *J. Phys. Chem. C* **2013**, *117*, 9623-9632.
[14] I. Kondrasenko, K.-y. Chung, Y.-T. Chen, J. Koivistoinen, E. V. Grachova, A. J. Karttunen, P.-T. Chou, I. O. Koshevoy, *J. Phys. Chem. C* **2016**, *120*, 12196-12206.
[15] E. Aguiló, A. J. Moro, M. Outis, J. Pina, D. Sarmento, J. S. Seixas de Melo, L. Rodríguez, J. C. Lima, *Inorg. Chem.* **2018**, *57*, 13423-13430.
[16] J. R. Shakirova, M. Shimada, D. A. Olisov, G. L. Starova, H. Nishihara, S. P. Tunik, *Z. Anorg. Allg. Chem.* **2018**, *644*, 308-316.
[17] A. Belyaev, I. Kolesnikov, A. S. Melnikov, V. V. Gurzhiy, S. P. Tunik, I. O. Koshevoy, *New J. Chem.* **2019**, *43*, 13741-13750.
[18] J. J. Mihaly, A. T. Phillips, D. J. Stewart, Z. M. Marsh, C. L. McCleese, J. E. Haley, M. Zeller, T. A. Grusenmeyer, T. G. Gray, *Phys. Chem. Chem. Phys.* **2020**, *22*, 11915-11927.
[19] I. D. Strelnik, V. V. Sizov, N. V. Gurzhiy, A. S. Melnikov, I. E. Kolesnikov, E. I. Musina, A. A. Karasik, E. V. Grachova, *Inorg. Chem.* **2020**, *59*, 244-253.
[20] V. W.-W. Yam, S. W.-K. Choi, K.-K. Cheung, *Organometallics* **1996**, *15*, 1734-1739.
[21] W. J. Hunks, M.-A. MacDonald, M. C. Jennings, R. J. Puddephatt, *Organometallics* **2000**, *19*, 5063-5070.
[22] X. He, E. C.-C. Cheng, N. Zhu, V. W.-W. Yam, *Chem. Commun.* **2009**, 4016-4018.
[23] M. El Sayed Moussa, H. Chen, Z. Wang, M. Srebro-Hooper, N. Vanthuyne, S. Chevance, C. Roussel, J. A. G. Williams, J. Autschbach, R. Réau, Z. Duan, C. Lescop, J. Crassous, *Chem. Eur. J.* **2016**, 6075-6086.
[24] A. Chu, F. Ka-Wah Hau, V. Wing-Wah Yam, *Chem. Eur. J.* **2017**, *23*, 11076-11084.
[25] F. C.-M. Leung, V. W.-W. Yam, *Eur. J. Inorg. Chem.* **2017**, 5271-5278.
[26] F. K.-W. Hau, K.-L. Cheung, N. Zhu, V. W.-W. Yam, *Org. Chem. Front.* **2019**, *6*, 1205-1213.
[27] L. Rodríguez, M. Ferrer, R. Crehuet, J. Anglada, J. C. Lima, *Inorg. Chem.* **2012**, *51*, 7636-7641.
[28] A. Pinto, N. Svahn, J. C. Lima, L. Rodríguez, *Dalton Trans.* **2017**, *46*, 11125-11139.
[29] M. Głodek, S. Pawlędzio, A. Makal, D. Plażuk, *Chem. Eur. J.* **2019**, *25*, 13131-13145.
[30] S.-K. Yip, E. C.-C. Cheng, L.-H. Yuan, N. Zhu, V. W.-W. Yam, *Angew. Chem. Int. Ed.* **2004**, *43*, 4954-4957.
[31] V. Cámara, N. Barquero, D. Bautista, J. Gil-Rubio, J. Vicente, *Chem. Eur. J.* **2015**, *21*, 1992-2002.
[32] E. Aguiló, R. Gavara, C. Baucells, M. Guitart, J. C. Lima, J. LLorca, L. Rodríguez, *Dalton Trans.* **2016**, *45*, 7328-7339.
[33] K. T. Chan, G. S. M. Tong, W.-P. To, C. Yang, L. Du, D. L. Phillips, C.-M. Che, *Chem. Sci.* **2017**, *8*, 2352-2364.
[34] V. W.-W. Yam, E. C.-C. Cheng, *Chem. Soc. Rev.* **2008**, *37*, 1806-1813.
[35] A. V. Paderina, I. O. Koshevoy, E. V. Grachova, *Dalton Trans.* **2021**, *50*, 6003-6033.
[36] J. C. Lima, L. Rodríguez, *Chem. Soc. Rev.* **2011**, 5442-5456.
[37] V. W.-W. Yam, V. K.-M. Au, S. Y.-L. Leung, *Chem. Rev.* **2015**, *115*, 7589-7728.
[38] E. Y.-H. Hong, V. W.-W. Yam, *ACS Appl. Mater. Interfaces* **2017**, *9*, 2616-2624.
[39] X. He, V. W.-W. Yam, *Coord. Chem. Rev.* **2011**, *255*, 2111-2123.
[40] Y.-P. Zhou, E.-B. Li, J. Wang, H.-Y. Chao, *Inorg. Chem.* **2013**, *52*, 8629-8637.
[41] E. E. Langdon-Jones, D. Lloyd, A. J. Hayes, S. D. Wainwright, H. J. Mottram, S. J. Coles, P. N. Horton, S. J. A. Pope, *Inorg. Chem.* **2015**, *54*, 6606-6615.
[42] R. Gavara, E. Aguiló, J. Schur, J. Llorca, I. Ott, L. Rodríguez, *Inorg. Chim. Acta*, **2016**, 446, 189-197.
[43] J. Sansévérino, J.-C. Chambron, E. Aubert, E. Espinosa, *J. Org. Chem.* **2011**, *76*, 1914-1917.
[44] F. Brégier, S. Karuppannan, J.-C. Chambron, *Eur. J. Org. Chem.* **2012**, 1920-1925.
[45] F. Brégier, J. Lavalle, J.-C. Chambron, *Eur. J. Org. Chem.* **2013**, 2666-2671.
[46] F. Brégier, E. Aubert, E. Espinosa, J.-C. Chambron, *ChemistrySelect* **2016**, *1*, 2389-2395.
[47] A. Collet, *Tetrahedron* **1987**, *43*, 5725-6759.
[48] A. Collet, J.-P. Dutasta, B. Lozach, J. Canceill, *Top. Curr. Chem.* **1993**, 165, 103-129.
[49] G. El-Aye, K. T. Holman, in *Comprehensive Supramolecular Chemistry II* (Eds. J. L. Atwood, G. W. Gokel, L. Barbour), Elsevier, Amsterdam, **2017**, vol. 6, p. 199.
[50] D. Zhang, A. Martinez, J.-P. Dutasta, *Chem. Rev.* **2017**, *117*, *6*, 4900-4942.
[51] M. J. Hardie, *Chem. Soc. Rev.* **2010**, *39*, 516-527.
[52] J. J. Henkelis, M. J. Hardie, *Chem. Commun.* **2015**, *51*, 11929-11943.
[53] N. J. Cookson, J. M. Fowler, D. P. Martin, J. Fisher, J. J. Henkelis, T. K. Ronson, F. L. Thorp-Greenwood, C. E. Willans, M. J. Hardie, *Supramol. Chem.* **2018**, *30*, 255-266.
[54] C. Givelet, J. Sun, D. Xu, T. J. Emge, A. Dhokte, R. Warmuth, *Chem. Commun.* **2011**, *47*, 4511-4513.
[55] F. Brégier, O. Hudeček, F. Chaux, M.-J. Penouilh, J.-C. Chambron, P. Lhoták, E. Aubert, E. Espinosa, *Eur. J. Org. Chem.* **2017**, 3795-3811.
[56] A. Schaly, Y. Rousselin, J.-C. Chambron, E. Aubert, E. Espinosa, *Eur. J. Inorg. Chem.* **2016**, 832-843.
[57] A. Schaly, M. Meyer, J.-C. Chambron, M. Jean, N. Vanthuyne, E. Aubert, E. Espinosa, N. Zorn, E. Leize-Wagner, *Eur. J. Inorg. Chem.* **2019**, 2691-2706.
[58] X.-N. Han, J.-M. Chen, Z.-T. Huang, Q.-Y. Zheng, *Eur. J. Org. Chem.* **2012**, 6895-6903.
[59] L. Peyrard, M.-L. Dumartin, S. Chierici, S. Pinet, G. Jonusauskas, P. Meyrand, I. Gosse, *J. Org. Chem.* **2012**, *77*, 7023-7027.
[60] L. Erieau-Peyrard, C. Coiffier, P. Bordat, D. Bégué, S. Chierici, S. Pinet, I. Gosse, I. Baraille, R. Brown, *Phys. Chem. Chem. Phys.* **2015**, *17*, 4168-4174.
[61] N. Fantozzi, R. Pétuya, A. Insuasty, A. Long, S. Lefevre, A. Schmitt, V. Robert, J.-P. Dutasta, I. Baraille, L. Guy, E. Genin, D. Bégué, A. Martinez, S. Pinet, I. Gosse, *New J. Chem.* **2020**, *44*, 11853-11860.
[62] D. Zhang, G. Gao, L. Guy, V. Robert, J.-P. Dutasta, A. Martinez, *Chem. Commun.* **2015**, *51*, 2679-2682.
[63] V. E. Pritchard, D. R. Martir, S. Oldknow, S. Kai, S. Hiraoka, N. J. Cookson, E. Zysman-Colman, M. J. Hardie, *Chem. Eur. J.* **2017**, *23*, 6290-6294.

[64] S. Oldknow, D. R. Martir, V. E. Pritchard, M. A. Blitz, C. W. G. Fishwick, E. Zysman-Colman, M. J. Hardie, *Chem. Sci.* **2018**, *9*, 8150-8159.

[65] A. Long, E. Antonetti, A. Insuasty, S. Pinet, I. Gosse, V. Robert, J.-P. Dutasta, A. Martinez, *J. Org. Chem.* **2020**, *85*, 6400-6407.

[66] D. L. Musso, M. J. Clarke, J. L. Kelley, G. E. Boswell, G. Chen, *Org. Biomol. Chem.* **2003**, *1*, 498-506.

[67] R. J. Cross, M. F. Davidson, *J. Chem. Soc. Dalton Trans.* **1986**, 411-414.

[68] W.-Y. Wong, Y. Guo, C.-L Ho, *J. Inorg. Organomet. Polym.* **2009**, *19*, 46-54.

[69] G. E. Coates, C. Parkin, *J. Chem. Soc.* **1962**, 3220-3226.

[70] S.-Y. Poon, W.-Y. Wong, K.-W. Cheah, J.-X. Shi, *Chem. Eur. J.* **2006**, *12*, 2550-2563.

[71] Q. Y. Hu, W. X. Lu, H. D. Tang, H. H. Y. Sung, T. B. Wen, I. D. Williams, G. K. L. Wong, Z. Lin, G. Jia, *Organometallics* **2005**, *24*, 3966-3973.

[72] W.-Y. Wong, S.-Y. Poon, *J. Inorg. Organomet. Polym.* **2008**, *18*, 155-162.

[73] W. Lu, N. Zhu, C.-M. Che, *J. Am. Chem. Soc.* **2003**, *125*, 16081-16088.

[74] W. Lu, N. Zhu, C.-M. Che, *J. Organomet.* Chem. **2003**, *670*, 11-16.

[75] Y. Cohen, L. Avram, L. Frish, *Angew. Chem. Int. Ed.* **2005**, *44*, 520-554.

[76] A. Macchioni, G. Ciancaleoni, C. Zuccaccia, D. Zuccaccia, *Chem. Soc. Rev.* **2008**, *37*, 479-489.

[77] B. M. Schulze, D. L. Watkins, J. Zhang, I. Ghiviriga, R. K. Castellano, *Org. Biomol. Chem.* **2014**, *12*, 7932-7936.

[78] This seems paradoxical, because alkynyl complexes are known to be acid-sensitive.

[79] C. Kowala, J. M. Swan, *Aust. J. Chem.* **1966**, *19*, 547-664.

[80] P. G. Jones, G. M. Scheldrick, E. Hädicke, *Acta Cryst.* **1980**, *B36*, 2777-2779.

[81] F. Canales, C. Gimeno, A. Laguna, M. D. Villacampa, *Inorg. Chim. Acta* **1996**, *244*, 95-103.

[82] A. Collet, G. Gottareli, *Croat. Chem. Acta* **1989**, *62*, 279-292.

[83] X.-X. Lu, C.-K. Li, E. C.-C. Cheng, N. Zhu, V. W.-W. Yam, *Inorg. Chem.* **2004**, *43*, 2225-2227.

[84] T. Brotin, R. Barbe, M. Darzac, J.-P. Dutasta, *Chem. Eur. J.* **2003**, *9*, 5784-5792.

[85] T. Brotin, N. Vanthuyne, D. Cavagnat, L. Ducasse, T. Buffeteau, *J. Org. Chem.* **2014**, *79*, 6028-6036.

[86] W.-Y. Wong, K.-H. Choi, G.-L. Lu, J.-X. Shi, P.-Y. Lai, S.-M. Chan, Z. Lin, *Organometallics* **2001**, *20*, 5446-5454.

[87] C.-C. Hsu, C.-C. Lin, P.-T. Chou, C.-H. Lai, C.-W. Hsu, C.-H. Lin, Y. Chi, *J. Am. Chem. Soc.* **2012**, *134*, 7715-7724.

[88] G. Mie, *Ann. Physik* **1908**, *25*, 377-445.

[89] Using (–)-**1**, we checked that the nanoparticles were molecular aggregates rather than gold nanoparticles by running the ^{1}H NMR spectrum of a solution of (–)-**1** in $CDCl_3$ obtained after dissolution of (–)-**1** in $CHCl_3$/MeOH 1:99 followed by solvent removal and drying (Figures S83-S84).

[90] (a) D. Xiao, W. Yang, J. Yao, L. Xi, X. Yang, Z. Shuai, *J. Am. Chem. Soc.* **2004**, *126*, 15439-15444; (b) Y. Zhang, A. Peng, J. Wang, W. Yang, J. Yao, *J. Photochem. Photobiol. A: Chemistry* **2006**, *181*, 94-98; (c) H. Yao, H. Sasahara, K. Kimura, *Chem. Mater.* **2011**, *23*, 913-922; (d) M. Li, C. Zhang, L. Fang, L. Shi, Z. Tang, H.-Y. Lu, C.-F. Chen, *ACS Appl. Mater. Interfaces* **2018**, *10*, 8225-8230.

[91] D. J. Gordon, *Biochemistry* **1972**, *11*, 413-420.

[92] M. I. Bruce, B. K. Nicholson, O. B. Shawkataly in *Inorganic Syntheses* (Ed.: H. D. Kaesz), Wiley-VCH, Weinheim, **1986**, p. 324.

Entry for the Table of Contents

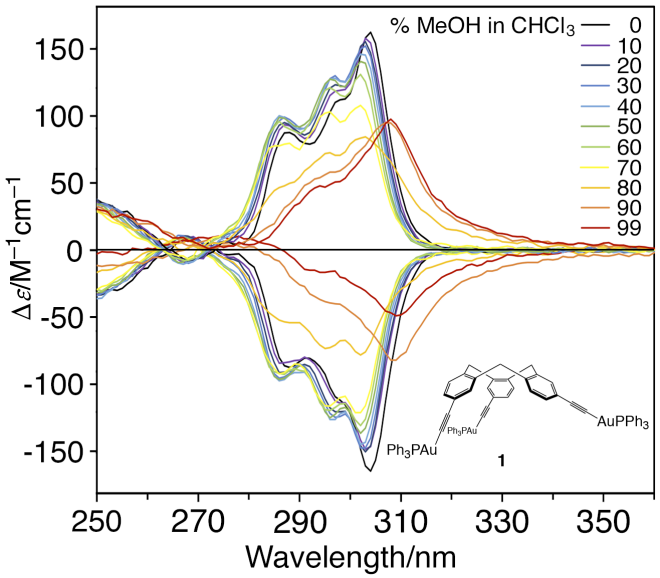

Alkynylgold(I) C_3-symmetric complexes bearing triphenyl (**1**) and trialkyl phosphine ligands (**2** and **3**) were synthesized and studied. In $CHCl_3$/MeOH mixtures **1** and **2** showed an AIE effect at 540 nm, probably originating from aurophilic interactions. **3** showed AIE only in nearly pure MeOH and in the solid state. The aggregation of optically pure **1** started at lower MeOH content than (±)-**1**, indicating that the latter gave racemates rather than conglomerates.